Article

SOURCE DATA | TRANSPARENT PROCESS | OPEN ACCESS

THE EMBO JOURNAL

Suppression of the HSF1-mediated proteotoxic stress response by the metabolic stress sensor AMPK

Siyuan Dai[1,†], Zijian Tang[1,2,†], Junyue Cao[1,†], Wei Zhou[1,†], Huawen Li[1], Stephen Sampson[1] & Chengkai Dai[1,*]

Abstract

Numerous extrinsic and intrinsic insults trigger the HSF1-mediated proteotoxic stress response (PSR), an ancient transcriptional program that is essential to proteostasis and survival under such conditions. In contrast to its well-recognized mobilization by proteotoxic stress, little is known about how this powerful adaptive mechanism reacts to other stresses. Surprisingly, we discovered that metabolic stress suppresses the PSR. This suppression is largely mediated through the central metabolic sensor AMPK, which physically interacts with and phosphorylates HSF1 at Ser121. Through AMPK activation, metabolic stress represses HSF1, rendering cells vulnerable to proteotoxic stress. Conversely, proteotoxic stress inactivates AMPK and thereby interferes with the metabolic stress response. Importantly, metformin, a metabolic stressor and popular anti-diabetic drug, inactivates HSF1 and provokes proteotoxic stress within tumor cells, thereby impeding tumor growth. Thus, these findings uncover a novel interplay between the metabolic stress sensor AMPK and the proteotoxic stress sensor HSF1 that profoundly impacts stress resistance, proteostasis, and malignant growth.

Keywords AMPK; HSF1; metformin; proteostasis; tumorigenesis
Subject Categories Metabolism; Molecular Biology of Disease; Protein Biosynthesis & Quality Control
DOI 10.15252/embj.201489062 | Received 21 May 2014 | Revised 6 October 2014 | Accepted 3 November 2014 | Published online 25 November 2014
The EMBO Journal (2015) 34: 275–293

See also: **CL Swan & L Sistonen** (February 2015)

Introduction

Organisms commonly encounter a wide variety of insults, both environmental and pathological. Many such insults, including heat shock, heavy-metal toxins, acidosis, ischemia/reperfusion, and oxidative damage, disturb cellular proteostasis and trigger the proteotoxic stress response (PSR), or heat shock response (Lindquist, 1986; Westerheide & Morimoto, 2005). This stress response is predominantly controlled by a transcription factor named heat shock factor 1 (HSF1) and is hallmarked by a drastic induction of heat shock proteins (HSPs) (Lindquist, 1986; Morimoto, 2008). HSPs are molecular chaperones, proteins that assist protein folding, trafficking, and degradation and thereby guard the proteome against the danger of misfolding and aggregation (Lindquist, 1986; Welch, 1991). Thus, this stress response plays an essential role in preserving proteostasis and enhancing survival in the face of such stressors, antagonizes neurodegeneration, and prolongs normal lifespan (Hsu *et al*, 2003; Balch *et al*, 2008; Dai *et al*, 2012a; Kondo *et al*, 2013; Lin *et al*, 2013; Pierce *et al*, 2013). Contrasting sharply with these broadly acclaimed benefits, our and others' recent studies have begun to reveal a surprising action of the HSF1-mediated stress response, whereby it is hijacked by malignant cells and facilitates oncogenesis (Dai *et al*, 2007, 2012a; Min *et al*, 2007; Meng *et al*, 2010; Jin *et al*, 2011; Scott *et al*, 2011).

Despite its evident importance in biology and human diseases, our understanding of the mechanisms through which this ancient adaptive stress response is regulated remains incomplete. In particular, little is known of how the PSR interacts with other cellular stress responses. One of such responses is the metabolic stress response that critically maintains cellular energy homeostasis. Metabolic stressors, through raising intracellular AMP/ATP ratios, instigate a low cellular energy state. By sensing increased AMP/ATP ratios, AMP-activated protein kinase (AMPK), a master metabolic regulator, becomes mobilized (Hardie, 2011). Mammalian AMPK is a protein complex comprising one catalytic α-subunit and two regulatory subunits: β and γ (Hardie, 2011). Upon activation, AMPK phosphorylates a wide array of downstream effectors to enhance ATP generation and reduce ATP expenditure (Hardie, 2011). This function of AMPK has proven crucial for cells to survive metabolic stress.

Herein, we report a novel interplay between the metabolic stress sensor AMPK and the proteotoxic stress sensor HSF1 and show that it has profound impacts on stress resistance, proteostasis, and tumor growth.

1 The Jackson Laboratory, Bar Harbor, ME, USA
2 Graduate Programs, Department of Molecular & Biomedical Sciences, The University of Maine, Orono, ME, USA
*Corresponding author. Tel: +1 207 288 6927; Fax: +1 207 288 6078; E-mail: Chengkai.Dai@jax.org
†These authors contributed equally to this work

Results

Metformin suppresses the HSF1-mediated PSR

In order to infer small molecules that potentially modulate the HSF1-mediated PSR, we queried the Connectivity Map (www.broadinstitute.org/cmap), a collection of gene expression profiles from human cells treated with bioactive molecules (Lamb *et al*, 2006), with a gene signature that was identified in human breast cancer cells following *HSF1* knockdown (Santagata *et al*, 2013). As expected, perturbagens known to activate HSF1, including the proteasome inhibitor MG-262 and HSP90 inhibitors (alvespimycin, tanespimycin, and monorden), generate gene expression patterns opposite to the query HSF1-inactivation gene signature (Fig 1A). In contrast, two translation inhibitors, cephaeline and emetine, generate expression patterns enriched for the query gene signature, congruent with their roles in suppressing HSF1 activation (Santagata *et al*, 2013). Intriguingly, metformin, a metabolic stressor and the most frequently prescribed medication for type II diabetes mellitus (T2D) worldwide (Dowling *et al*, 2011), also provokes gene expression changes concordant with HSF1 inactivation (Fig 1A).

Next, we experimentally verified the metformin-mediated suppression of the PSR by testing the ability of metformin to suppress heat shock-induced HSP expression. For HSP expression, we used an NIH3T3 reporter cell line that stably expresses a GFP-firefly luciferase fusion controlled by the human *HSP70B* (*HSPA6*) promoter (Dai *et al*, 2012a). As expected, heat shock-induced GFP expression in phosphate-buffered saline (PBS)-treated cells and metformin markedly blocked this induction (Fig 1B). Metformin also impaired induction of endogenous HSP72 and HSP25 proteins (Fig 1C), two classic stress-inducible HSPs. Congruent with transcriptional suppression by metformin, induction of *Hsp72* (*Hspa1a*) and *Hsp25* (*Hspb1*) mRNAs by heat shock was markedly impaired in metformin-treated cells compared to control cells (Fig 1D and E). While these notable effects were achieved using 10 mM metformin, a similar pattern of changes, albeit to a lesser extent (Supplementary Fig S1A and B), was also observed for 10 μM metformin, a concentration comparable to that found in the blood of T2D patients (Sum *et al*, 1992; Lalau *et al*, 2011; Dowling *et al*, 2012). Importantly, this defect in the PSR was not due to impaired cell viability following metformin treatment (Fig 1F).

To demonstrate impaired HSF1 activation, we directly examined HSF1–DNA binding. To accomplish this, we developed a new enzyme-linked immunosorbent assay (ELISA)-based technique to measure HSF1–DNA binding capability (Fig 1G, left panel). In this assay, nuclear HSF1 proteins competent for DNA binding are captured by ideal heat shock element (HSE) oligonucleotides that are pre-immobilized on a microtiter plate through biotin–avidin interactions. Subsequently, a specific primary antibody recognizes the DNA-bound HSF1 proteins, followed by detection with secondary antibodies. As expected, HSF1–DNA binding was markedly increased following heat shock (Supplementary Fig S1C); however, metformin evidently blocked this increase (Fig 1G, right panel).

While our new method is quantitative and high-throughput, it requires, similar to the prevailing chromatin IP (ChIP) technique, a large amount of DNA and provides only average values for a given cell population. To provide more detailed information on HSF1–DNA binding, we adapted the newly emerged proximity ligation assay (PLA) technique to visualize endogenous physical associations between HSF1 and genomic DNAs at the single-cell level. By means of two species-specific secondary antibodies conjugated with oligonucleotides, PLA converts protein–protein interactions in proximity into DNA signals (Clausson *et al*, 2011). We extended this technique to detect HSF1–DNA interactions *in situ* by utilizing a mouse anti-double-stranded DNA antibody in conjunction with a rabbit anti-HSF1 antibody (Fig 1H). The specificity of antibodies was validated by standard immunostaining. In HEK293T cells, the DNA antibody generated similar staining patterns with and without heat shock (Supplementary Fig S1D). This staining largely overlaid with that of the DNA dye DAPI, indicating a predominant DNA

Figure 1. Metformin suppresses the HSF1-mediated PSR.

A The connectivity map suggests that metformin generates a gene expression pattern concordant with HSF1 inactivation. Perturbagens inducing and reversing the biological state encoded in the query signature are assigned positive and negative enrichment scores, respectively.

B Following treatment with 10 mM metformin overnight, NIH3T3 reporter cells were heat-shocked at 43°C for 30 min and recovered at 37°C for 5 h. GFP induction was quantitated by flow cytometry. HS: heat shock.

C Individual proteins in reporter cells treated with and without 10 mM metformin overnight were detected by immunoblotting.

D, E Following heat shock and recovery for 4 h, mRNA levels in reporter cells treated with and without 10 mM metformin overnight were quantitated by qRT–PCR (mean ± SD, $n = 3$, Student's *t*-test, $^{**}P < 0.01$, $^{***}P < 0.001$). β-actin was used as the internal control.

F Reporter cells were treated with 10 mM metformin overnight, and viability was measured using Guava ViaCount® reagents (mean ± SD, $n = 5$, n.s., not significant, Student's *t*-test).

G Left panel, graphic depiction of the ELISA-based DNA binding assay. HSE: heat shock element. Right panel: Immediately following heat shock at 43°C for 30 min, nuclear proteins of the reporter cells treated with and without 10 mM metformin were extracted for assay (mean ± SD, $n = 3$, Student's *t*-test, $^{**}P < 0.01$, $^{***}P < 0.001$). Experimental details are described in Materials and Methods.

H Graphic depiction of the adapted PLA. A pair of primary antibodies recognizes DNA-bound HSF1s and dsDNAs, respectively.

I HEK293T cells stably expressing a scramble or *HSF1*-targeting shRNA were treated with 10 mM metformin overnight and heat-shocked at 43°C for 30 min. Cells were fixed for PLA to detect HSF1–DNA interactions. Experimental details are described in Materials and Methods. Scale bars: 50 μm for low magnification and 10 μm for high magnification.

J Immediately following heat shock, cytoplasmic and nuclear proteins of the reporter cells treated with and without 10 mM metformin were extracted for immunoblotting. LDH and Lamin A/C were used as cytoplasmic and nuclear markers, respectively. C: cytoplasm; N: nucleus.

K Reporter mice (ventral side shown) were pre-treated with metformin for 3 days, 2 mg/mouse/day, via i.p. injection. Following a single i.p. injection of velcade (5 mg/kg) and recovery for 6 h, whole-body luciferase activities were quantitated by bioluminescence imaging. The photon flux of each mouse was expressed as photon/s/cm^2/steradian (right panel, mean ± SD, $n = 3$, one-way ANOVA, $^{*}P < 0.05$; $^{**}P < 0.01$).

Source data are available online for this figure.

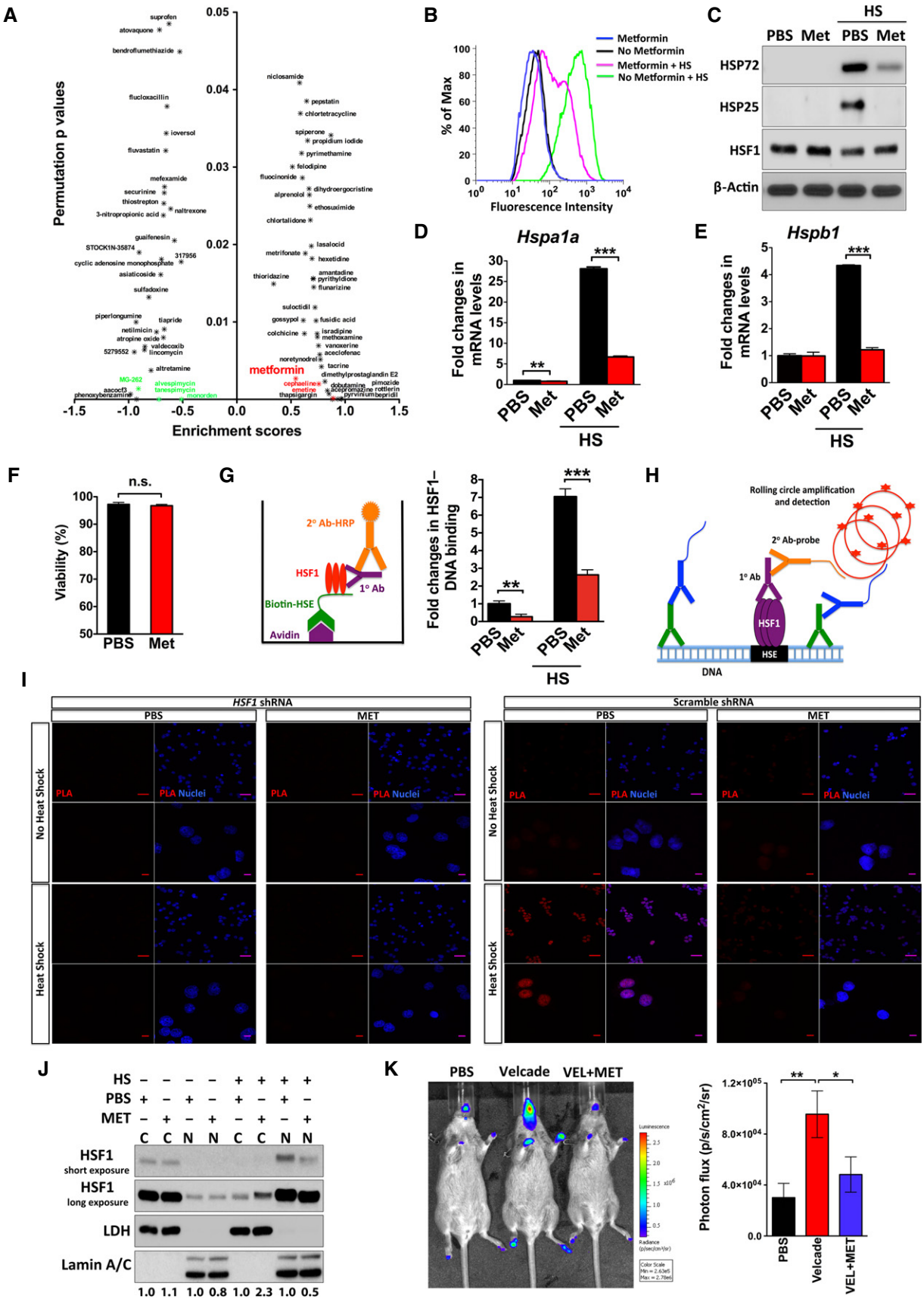
A
Permutation p values
Enrichment scores
suprofen
atovaquone
bendroflumethiazide
flucloxacillin
ioversol
fluvastatin
mefexamide
securinine
thiostrepton
3-nitropropionic acid
naltrexone
guaifenesin
STOCK1N-35874
317956
cyclic adenosine monophosphate
asiaticoside
sulfadoxine
piperlongumine
tiapride
netilmicin
atropine oxide
5279552
valdecoxib
lincomycin
altretamine
MG-262
aacocf3
phenoxybenzamine
alvespimycin
tanespimycin
monorden
niclosamide
pepstatin
chlortetracycline
spiperone
propidium iodide
pyrimethamine
felodipine
fluocinonide
dihydroergocristine
alprenolol
ethosuximide
chlortalidone
lasalocid
metrifonate
hexetidine
thioridazine
amantadine
pyrithyldione
flunarizine
suloctidil
gossypol
fusidic acid
colchicine
isradipine
methoxamine
vanoxerine
aceclofenac
noretynodrel
tacrine
metformin
dimethylprostaglandin E2
cephaeline
emetine
thapsigargin
dobutamine
pimozide
rottlerin
pyrvinium
bepridil
B
Metformin
No Metformin
Metformin + HS
No Metformin + HS
% of Max
Fluorescence Intensity
C
HS
PBS Met PBS Met
HSP72
HSP25
HSF1
β-Actin
D
Hspa1a
Fold changes in mRNA levels
PBS Met PBS Met
HS
E
Hspb1
Fold changes in mRNA levels
PBS Met PBS Met
HS
F
n.s.
Viability (%)
PBS Met
G
2° Ab-HRP
HSF1
1° Ab
Biotin-HSE
Avidin
Fold changes in HSF1–DNA binding
PBS Met PBS Met
HS
H
Rolling circle amplification and detection
2° Ab-probe
1° Ab
HSF1
HSE
DNA
I
HSF1 shRNA
Scramble shRNA
PBS
MET
No Heat Shock
Heat Shock
PLA
PLA Nuclei
J
HS
PBS
MET
C C N N C C N N
HSF1 short exposure
HSF1 long exposure
LDH
Lamin A/C
1.0 1.1 1.0 0.8 1.0 2.3 1.0 0.5
K
PBS Velcade VEL+MET
Photon flux (p/s/cm²/sr)
PBS
Velcade
VEL+MET

Figure 1.

labeling irrespective of heat shock. Importantly, this staining was markedly reduced following DNase treatment (Supplementary Fig S1E), indicating specific DNA labeling. As a negative control, HEK293T cells stably expressing *HSF1*-targeting shRNAs did not display notable HSF1 staining (Supplementary Fig S1F). Congruently, no specific PLA signals were detected in these *HSF1*-deficient cells (Fig 1I, left panel). In cells expressing scramble shRNAs and without heat shock, only sporadic PLA signals, manifested as distinct nuclear foci, were observed (Fig 1I, right panel), indicating basal constitutive HSF1 activation. In contrast, heat shock greatly increased these signals, demonstrated by numerous bright nuclear foci (Fig 1I, right panel). Importantly, metformin potently blocked this increase (Fig 1I, right panel), demonstrating impaired *in vivo* HSF1–DNA binding by metformin.

HSF1 activation is a multi-step process, involving phosphorylation, nuclear translocation, and DNA binding. Next, we investigated whether metformin affected HSF1 nuclear translocation, a prerequisite for its DNA binding. As expected, heat shock caused most HSF1 proteins to translocate from the cytoplasm to the nucleus (Fig 1J). Importantly, metformin impeded this translocation (Fig 1J). Thus, metformin impairs HSF1–DNA binding at least in part through blockade of its nuclear translocation.

To determine whether metformin impairs the PSR at the organismal level, we utilized transgenic mice that express dual reporter genes, firefly luciferase and EGFP, both controlled by the mouse *Hsp72* promoter (O'Connell-Rodwell *et al*, 2008). When analyzed with bioluminescence imaging, these mice enable noninvasive surveillance of the PSR *in vivo*. Under non-stress conditions, these reporter mice exhibited basal luciferase activities in mouth and limbs (Fig 1K; Supplementary Fig S1G). As expected, challenge with the proteasome inhibitor velcade, a potent proteotoxic stressor, markedly increased whole-body luciferase activities. However, pretreatment with metformin impaired the velcade-induced elevation of luciferase activities (Fig 1K; Supplementary Fig S1G). Together, these results indicate that metformin suppresses the PSR through inactivation of HSF1.

AMPK negatively regulates HSF1 activation via phosphorylation

We next sought to elucidate the molecular mechanisms by which metformin inactivates HSF1. Through diminishment of mitochondrial ATP production, metformin activates AMPK, a key cellular sensor of metabolic stress (El-Mir *et al*, 2000). This activation is known to mediate numerous effects of metformin (Kahn *et al*, 2005). However, it has also been reported that metformin inhibits mTORC1 independently of AMPK (Kalender *et al*, 2010).

We first asked whether mTORC1 inhibition by metformin mediates HSF1 suppression. To address this, we examined induction of *Hsp* genes in cells treated with rapamycin, a specific mTOR inhibitor. Successful inhibition of mTORC1 by rapamycin was evidenced by a marked reduction of S6K1 phosphorylation (Supplementary Fig S2A). In stark contrast to metformin, in our experiments, rapamycin enhanced *Hsp* induction by heat shock (Supplementary Fig S2B and C), arguing against mTORC1 inhibition as a primary cause of HSF1 suppression by metformin. This result somewhat contrasts with a recent report, indicating that rapamycin suppressed HSF1 activation (Chou *et al*, 2012). Surprisingly, our results showed that whereas high doses of rapamycin suppressed HSF1, low doses activated HSF1 (unpublished observations), suggesting indirect regulation of HSF1 by mTORC1. As expected, metformin induced AMPK activation, evidenced by elevated Thr172 phosphorylation of AMPKα (Supplementary Fig S2A; Hawley *et al*, 1996). Moreover, two other mechanistically distinct AMPK activators, A-769662 and aminoimidazole carboxamide ribonucleotide (AICAR) (Corton *et al*, 1995; Göransson *et al*, 2007), also impaired the PSR (Fig 2A and B; Supplementary Fig S2D). A-769662 is a direct and specific AMPK activator, causing phosphorylation of the well-characterized AMPK substrate acetyl-CoA carboxylase (ACC) (Fig 2C; Göransson *et al*, 2007). These results suggest AMPK as a common mediator of HSF1 suppression.

To directly test this, we conditionally deleted the two *Ampkα* isoforms, *α1* and *α2*, in mouse embryonic fibroblasts (MEFs) through adenoviral Cre recombinase (Fig 2D). Compared to GFP transduction, Cre transduction in $Ampk\alpha1/2^{fl/fl}$ MEFs not only enhanced *Hsp* induction by heat shock but also markedly blocked metformin-induced *Hsp* suppression (Fig 2E and F), indicating the necessity of AMPK for metformin-mediated HSF1 inactivation. The incomplete blockade of metformin effect was likely due to residual AMPKα proteins (Fig 2D) and/or AMPK-independent mechanisms of metformin. To determine the sufficiency of AMPK activation for HSF1 suppression, we activated AMPK signaling through expression of a GST-tagged constitutively active mutant of the α1-subunit, $AMPK\alpha^{CA}$ (Egan *et al*, 2011). AMPK activation was evidenced by elevated phosphorylation of RAPTOR, a known cellular substrate for AMPK (Gwinn *et al*, 2008), at Ser792 (Supplementary Fig S2E). Under both basal and heat shock conditions, this mutant impaired activation of the HSF1 reporter (Fig 2G), demonstrating that AMPK activation alone is sufficient to repress the transcriptional activity of HSF1. Together, these results indicate a negative regulation of the PSR by AMPK.

We reasoned that AMPK might directly phosphorylate HSF1. To test this, we first examined potential physical interactions between AMPK and HSF1 by co-immunoprecipitation (co-IP). As a positive control, while some endogenous ACC proteins were co-precipitated with endogenous AMPKα in MEFs under basal conditions, metformin markedly enhanced this co-IP (Fig 2H). Importantly, in a similar pattern, endogenous HSF1 proteins were also co-precipitated with AMPKα (Fig 2H). In HEK293T cells, exogenous FLAG-HSF1 proteins were also co-precipitated with GST-$AMPK\alpha^{CA}$ (Supplementary Fig S2F), indicating specific *in vivo* physical AMPK–HSF1 interactions. This interaction was then confirmed *in situ* by PLA. Using a rabbit antibody recognizing Thr172-phosphorylated AMPKα in conjunction with a mouse monoclonal anti-HSF1 antibody, we visualized endogenous AMPK–HSF1 interactions in $Hsf1^{+/+}$ MEFs. $Hsf1^{-/-}$ MEFs served as negative controls. As expected, no specific PLA signals were observed in $Hsf1^{-/-}$ MEFs, irrespective of metformin treatment (Fig 2I). While only faint signals were detected in $Hsf1^{+/+}$ cells treated with PBS, metformin treatment markedly augmented these signals (Fig 2I), indicating a specific and inducible interaction between endogenous HSF1 and AMPK proteins.

We next asked whether AMPK inactivates HSF1 through phosphorylation. The protein motif algorithm ScanSite (http://scansite.mit.edu/) predicted a potential phosphorylation site on HSF1 at serine 121 residue (Supplementary Fig S3A). To test this, we took advantage of a phosphorylation-specific antibody. The specificity of this antibody was validated using a phosphorylation-resistant mutant, $HSF1^{S121A}$, in *HSF1*-deficient HEK293T cells. This antibody

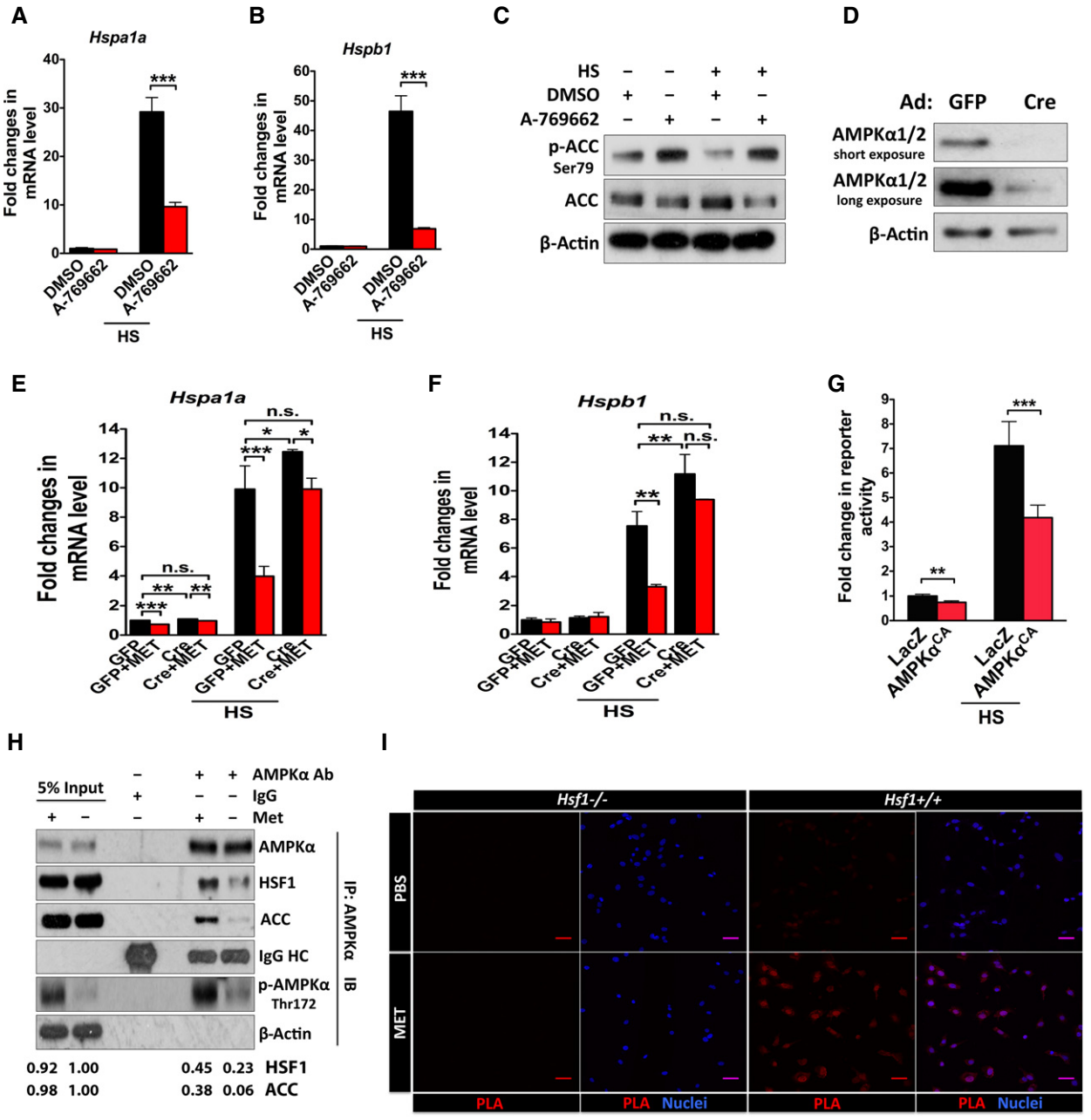

Figure 2. AMPK suppresses HSF1 activation through physical interaction.

A–C Reporter cells were treated with and without 1 μM A-769662 for 3 h followed by heat shock at 43°C for 30 min and recovery at 37°C for 5 h. *Hspa1a* and *Hspb1* mRNA levels were quantitated by qRT–PCR (mean ± SD, n = 3, Student's t-test, $^{***}P < 0.001$). ACC phosphorylation was detected by immunoblotting (C).

D–F Primary MEFs were derived from *Ampkα1*$^{fl/fl}$; *Ampkα2*$^{fl/fl}$ embryos and transduced with either adenoviral GFP or Cre to delete *Ampkα1/2 in vitro*. AMPKα levels were detected 4 days after transductions (D). Following viral transductions, *Hsp* mRNA levels were quantitated by qRT–PCR in MEFs with and without 10 mM metformin treatment overnight followed by 43°C heat shock for 30 min and recovery for 4 h (mean ± SD, n = 3, one-way ANOVA, n.s., not significant, $^{*}P < 0.05$, $^{**}P < 0.01$, $^{***}P < 0.001$).

G Transcriptional activities of HSF1 were measured by a dual reporter system consisting of two plasmids: the HSF1-dependent reporter pHSE-SEAP, in which ideal HSEs drive the expression of secreted alkaline phosphatase (SEAP), and the control reporter pCMV-*Gaussia* Luc, in which a CMV promoter drives the expression of secreted *Gaussia* luciferase. In HEK293T cells, either LacZ or GST-AMPKα1^{CA} plasmid was co-transfected with the two reporter plasmids. After 24 h, the transfected cells were heat-shocked at 44°C for 45 min. The culture supernatants were collected to measure SEAP and luciferase activities 24 h after heat shock. SEAP signals were normalized to *Gaussia* luciferase signals (mean ± SD, n = 5, Student's t-test, $^{**}P < 0.01$, $^{***}P < 0.001$).

H, I Following treatment with 10 mM metformin overnight, endogenous AMPKα and HSF1 proteins were co-precipitated using anti-AMPKα agarose conjugates from lysates of immortalized *Hsf1*$^{+/+}$ MEFs (H). HC: heavy chain. Endogenous HSF1-AMPKα interactions in immortalized *Hsf1*$^{+/+}$ and *Hsf1*$^{-/-}$ MEFs were visualized *in situ* by PLA (I). Experimental details are described in Materials and Methods. Scale bars: 50 μm.

Source data are available online for this figure.

readily detected exogenously expressed $HSF1^{WT}$ under basal conditions and metformin treatment enhanced this signal (Fig 3A). In contrast, the same antibody failed to detect exogenously expressed $HSF1^{S121A}$ mutants under both basal and metformin treatment conditions (Fig 3A). Moreover, this antibody did not detect specific signals in *Hsf1*$^{-/-}$ MEFs (Supplementary Fig S3B). Importantly, both *Ampkα1/2* deletion and *AMPKα1/2* knockdown largely blocked HSF1 Ser121 phosphorylation induced by metformin or A-769662 (Fig 3B; Supplementary Fig S3C), demonstrating the necessity of AMPK for this phosphorylation *in vivo*. Conversely, $AMPK\alpha^{CA}$ sufficed to induce Ser121 phosphorylation of $HSF1^{WT}$, but not $HSF1^{S121A}$ (Fig 3C). Previously, it was reported that MAPK-activated protein kinase 2 (MK2) could phosphorylate the same site (Wang *et al*, 2006). However, *MK2* knockdown failed to significantly block HSF1 Ser121 phosphorylation induced by metformin (Supplementary Fig S3D and E), indicating that MK2 is not important for this modification induced by metformin.

To address whether AMPK directly phosphorylates HSF1, we conducted *in vitro* kinase assays using immunoprecipitated AMPK complexes. Compared to IgG controls, precipitates of AMPKα antibodies weakly phosphorylated recombinant HSF1 proteins at Ser121 in the absence of AMP (Fig 3D). However, AMP markedly enhanced this phosphorylation and the AMPK inhibitor compound C blocked this event (Fig 3D; Zhou *et al*, 2001), indicating a specific action of AMPK. Congruent with its activation, AMPK complexes precipitated from metformin-treated cells more efficiently phosphorylated HSF1 (Fig 3D). Importantly, compared to its wild-type counterparts $HSF1^{S121A}$ mutants not only exhibited higher basal transcriptional activities but also were refractory to $AMPK\alpha^{CA}$- and metformin-mediated suppression (Fig 3E and F). In line with their transcriptional activities, $HSF1^{WT}$ and $HSF1^{S121A}$ exhibited differential DNA bindings (Fig 3G and H), demonstrating the importance of Ser121 phosphorylation to HSF1 suppression by AMPK. While both FLAG-$HSF1^{WT}$ and FLAG-$HSF1^{S121A}$ proteins were expressed at comparable levels in HEK293T cells under basal conditions, overnight metformin treatment slightly decreased $HSF1^{WT}$, but not $HSF1^{S121A}$ proteins (Supplementary Fig S3F and G). This reduction likely contributes to metformin-induced HSF1 suppression and suggests a role of Ser121 phosphorylation in HSF1 stability. Indeed, cycloheximide chase experiments revealed that metformin treatment for 24 h accelerated HSF1 turnover and S121A mutation markedly mitigated this effect (Supplementary Fig S3H). Interestingly, in contrast to metformin, $AMPK\alpha^{CA}$ expression did not reduce $HSF1^{WT}$ levels (Supplementary Fig S3F). These results suggest that Ser121 phosphorylation is necessary but not sufficient to destabilize HSF1 and that additional mechanisms may be involved in metformin-induced HSF1 instability. Despite no impacts on HSF1 expression, $AMPK\alpha^{CA}$ impaired constitutive nuclear translocation of $HSF1^{WT}$ in HEK293T cells, indicated by diminished nuclear–cytoplasmic ratio of HSF1 levels (Fig 3I). S121A mutation not only enhanced HSF1 nuclear translocation under basal conditions but also rendered HSF1 resistant to the effect of $AMPK\alpha^{CA}$ (Fig 3I). Similarly, while metformin impaired $HSF1^{WT}$ nuclear translocation, it exerted little effect on $HSF1^{S121A}$ mutants (Fig 3J). Thus, this defect in nuclear translocation due to Ser121 phosphorylation at least in part contributes to reduced HSF1–DNA binding. In summary, these results indicate that activated AMPK physically interacts with HSF1 and suppresses its activity primarily via Ser121 phosphorylation.

Metabolic stress suppresses the PSR

In response to metabolic stress, AMPK is mobilized to sustain cellular energy homeostasis and improve survival (Kahn *et al*, 2005). In light of the inactivation of HSF1 by AMPK that we discovered, we next asked whether metabolic stress impacts the cellular response to proteotoxic stress. To provoke metabolic stress, we applied either leucine or glucose deprivation to the NIH3T3 heat shock reporter cells described above. Similar to metformin treatment, deprivation of each nutrient suppressed GFP induction by heat shock (Fig 4A and B). This suppression was not due to impaired cell viability following nutrient deprivation (Supplementary Fig S4A and B). Mechanistically, nutrient deprivation impaired HSF1–DNA binding following heat shock (Fig 4C and D), thereby impairing HSP induction (Fig 4E and F). Congruent with diminished

Figure 3. AMPK phosphorylates Ser121 to inactivate HSF1.

A In HEK293T cells that stably express an shRNA targeting the 3′ UTR of human *HSF1*, $HSF1^{WT}$ or $HSF1^{S121A}$ was expressed. Following treatment with 10 mM metformin overnight, the levels of HSF1 phosphorylation at Ser121 were detected by immunoblotting using a specific phospho-HSF1 Ser121 antibody (A8041, Assay Biotechnology).

B Primary *Ampkα1*$^{fl/fl}$; *Ampkα2*$^{fl/fl}$ MEFs were transduced with adenoviral GFP or Cre. Following treatment with 10 mM metformin overnight or treatment with 10 μM A-769662 for 3 h, HSF1 Ser121 phosphorylation was examined by immunoblotting.

C $HSF1^{WT}$ or $HSF1^{S121A}$ was co-expressed with either GFP or GST-$AMPK\alpha^{CA}$ in *HSF1*-deficient HEK293T cells. HSF1 Ser121 phosphorylation was examined by immunoblotting.

D AMPK complexes were immunoprecipitated from HEK293T cells treated with and without 10 mM metformin overnight. Aliquots of AMPK complexes were incubated with 400 ng purified recombinant His-tagged HSF1 proteins with and without 100 μM AMP or 20 μM compound C (CC). HSF1 Ser121 phosphorylation was detected by immunoblotting.

E, F HSF1 activities were measured by the dual reporter system in *HSF1*-deficient HEK293T cells. Either FLAG-$HSF1^{WT}$ or FLAG-$HSF1^{S121A}$ was co-expressed with LacZ or $AMPK\alpha1^{CA}$ (E). Following expression of $HSF1^{WT}$ or $HSF1^{S121A}$, cells were treated with and without 10 mM metformin overnight (F) (mean ± SD, n = 5, one-way ANOVA, n.s., not significant, *$P < 0.05$, **$P < 0.01$, ***$P < 0.001$).

G, H FLAG-$HSF1^{WT}$ or FLAG-$HSF1^{S121A}$ plasmids were co-transfected with LacZ or $AMPK\alpha1^{CA}$ plasmids into *HSF1*-deficient HEK293T cells for 3 days (G). Following transfection with FLAG-$HSF1^{WT}$ or FLAG-$HSF1^{S121A}$ plasmids for 3 days, *HSF1*-deficient HEK293T cells were treated with and without 10 mM metformin overnight (H). Nuclear proteins were extracted to measure HSF1–DNA binding by the ELISA-based DNA binding assay using anti-FLAG antibodies (mean ± SD, n = 3, one-way ANOVA, n.s., not significant, *$P < 0.05$, **$P < 0.01$, ***$P < 0.001$).

I, J Following transfections and metformin treatment as described in (G) and (H), cytoplasmic and nuclear proteins were extracted for immunoblotting using anti-FLAG antibodies.

Source data are available online for this figure.

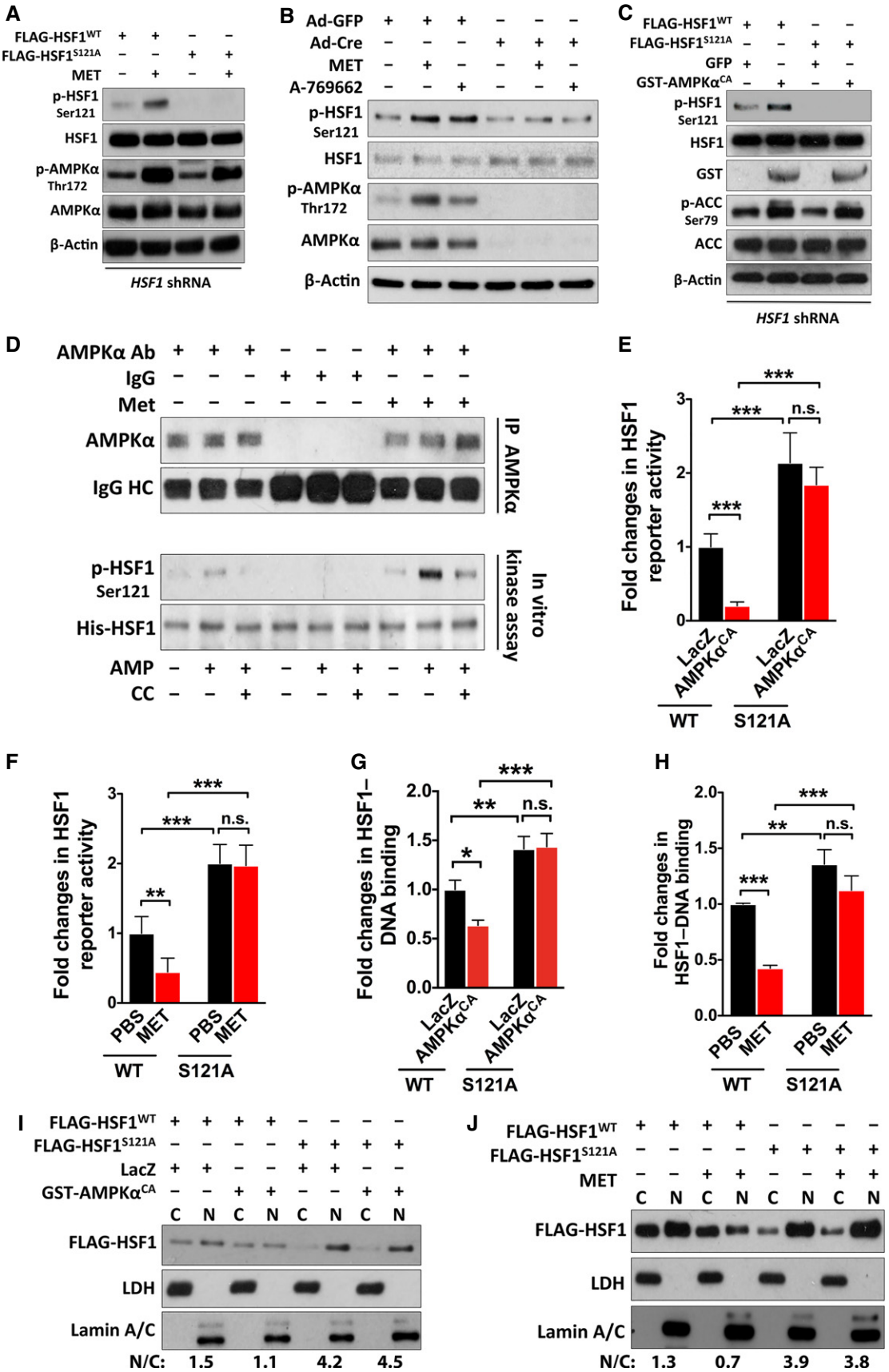

Figure 3.

protein-chaperoning capacity following nutrient deprivations, protein Lys48 polyubiquitination, a key modification targeting proteins for proteasomal degradation and a surrogate indicator of protein misfolding (Pickart & Eddins, 2004), was aggravated under both basal and heat shock conditions (Fig 4E and F). In stark contrast, both nutrient deprivations induced expression of BiP/GRP78 (Fig 4E and F), a key endoplasmic reticulum (ER) chaperone and marker of the unfolded protein response (UPR), which responds to ER stress (Walter & Ron, 2011). Together, these results indicate that nutrient deprivations trigger the UPR but, intriguingly, suppress the PSR. As expected, both nutrient deprivations induced AMPKα Thr172 phosphorylation in NIH3T3 and HEK293 cells (Fig 4G and H; Supplementary Fig S4C and D). Congruent with HSF1 phosphorylation by AMPK, both nutrient deprivations also induced HSF1 Ser121 phosphorylation (Fig 4G and H; Supplementary Fig S4C and D). Of note, 4-h leucine starvation was required to induce evident AMPK phosphorylation (Fig 4G; Supplementary Fig S4C). These findings not only agree with HSF1 inactivation by AMPK (Fig 2), but also suggest AMPK activation as a common mechanism underlying the inhibitory effect of metabolic stress on the PSR.

Suppression of HSF1 activation by nutrient deprivations was further confirmed in HEK293 cells. Importantly, *AMPKα1/2* knockdown not only elevated basal HSF1 activity but also reversed HSF1 suppression imposed by nutrient deprivations (Fig 4I and J). It has been known that AMPK activation inhibits mTORC1 (Gwinn *et al*, 2008). To determine whether mTORC1 inhibition following nutrient deprivations plays an important role in HSF1 inactivation, we measured HSF1 transcriptional activities under nutrient deprivations in the presence of high doses of rapamycin. While 500 nM rapamycin alone suppressed HSF1, combined nutrient deprivation further inactivated HSF1 (Supplementary Fig S4E), strongly suggesting that AMPK activation induced by nutrient deprivations is capable of suppressing HSF1 independently of mTORC1. Congruent with a direct regulatory mechanism, S121A mutation rendered HSF1 resistant to nutrient deprivation-mediated suppression (Fig 4K and L). Together, these results reveal that metabolic stress antagonizes the HSF1-mediated PSR, wherein AMPK activation plays an important role via phosphorylating HSF1 at Ser121.

Proteotoxic stress suppresses AMPK

In stark contrast to metabolic stress, our results revealed that heat shock markedly diminished AMPK Thr172 phosphorylation (Fig 5A and Supplementary Fig S5A). In parallel, HSF1 Ser121 phosphorylation was also reduced under heat shock (Fig 5A and Supplementary Fig S5A), suggesting AMPK inactivation. This was confirmed by *in vitro* kinase assays. Compared to AMPK complexes immunoprecipitated from cells without heat shock, complexes from heat-shocked cells exhibited markedly impaired capability to phosphorylate recombinant ACC1 proteins *in vitro* even in the presence of AMP (Fig 5B). Congruent with this defect, heat shock caused a specific reduction of γ2-subunit within immunoprecipitated AMPK complexes (Fig 5B). AMPKγ subunits play a critical role in binding AMP/ATP, and mutations in γ2-subunit are associated with cardiac hypertrophy (Blair *et al*, 2001; Hardie, 2011). To our surprise, 30-min heat shock sufficed to diminish total cellular γ2-subunits (Fig 5B). We reasoned that this reduction was likely due to protein instability. In support of this notion, an increase in γ2-subunit was detected in detergent-insoluble fractions of cellular protein extracts and a simultaneous decrease in this subunit was detected in detergent-soluble fractions (Fig 5C), suggesting oligomerization and/or aggregation of γ2-subunits under heat shock conditions. Thus, our results indicate that, at least through regulation of Thr172 phosphorylation of α-subunits and destabilization of γ-subunits, heat shock suppresses AMPK.

Given the pivotal role of AMPK in mediating the metabolic stress response, we were curious to know whether proteotoxic stress could interfere with cellular responses to metabolic stressors. Consistent with its inhibitory effect on AMPK, transient heat shock immediately proceeding nutrient deprivations significantly impaired induction of AMPK and ACC phosphorylation (Fig 5D and E), suggesting suppression of the metabolic stress response by heat shock.

We next asked whether attenuation of Ser121 phosphorylation during heat shock contributes to HSF1 activation. Compared to cells expressing $HSF1^{WT}$, cells expressing $HSF1^{S121A}$ exhibited elevated *HSP* mRNAs, HSF1–DNA binding, and reporter activities under both basal and heat shock conditions (Fig 5F–H and Supplementary Fig S5B). Under basal conditions, expression levels of $HSF1^{WT}$ and $HSF1^{S121A}$ were comparable and, therefore, heightened activity of $HSF1^{S121A}$ was at least in part due to its enhanced nuclear translocation (Supplementary Fig S5C and D). Following heat shock, both $HSF1^{WT}$ and $HSF1^{S121A}$ proteins slightly increased (Supplementary Fig S5C). Interestingly, $HSF1^{S121A}$ mutants increased more compared to $HSF1^{WT}$ (Supplementary Fig S5C), congruent with a role of Ser121 phosphorylation in HSF1 stability. This elevated protein levels may also contribute to heightened HSF1 activities in cells expressing $HSF1^{S121A}$ under heat shock conditions, in addition

Figure 4. Metabolic stress suppresses the PSR through AMPK.

A, B NIH3T3 reporter cells were cultured overnight in DMEM with and without leucine (A) or 4.5 g/l glucose (B). Following heat shock at 43°C for 30 min and recovery for 5 h, GFP induction was quantitated by flow cytometry.

C, D Nuclear proteins were extracted from reporter cells with and without nutrient deprivations overnight for the ELISA-based DNA binding assay (mean ± SD, $n = 3$, Student's *t*-test, $^*P < 0.05$, $^{**}P < 0.01$, $^{***}P < 0.001$).

E, F Following nutrient deprivations overnight, the reporter cells were heat-shocked at 43°C for 30 min and recovered overnight. Individual proteins were detected by immunoblotting.

G, H Reporter cells were subjected to nutrient starvation for the indicated time. AMPKα Thr172 and HSF1 Ser121 phosphorylation was measured by immunoblotting.

I, J HEK293T cells were sequentially transfected with control or *AMPKα1/2*-targeting siRNAs and dual HSF1 reporter plasmids. 24 h later, transfected cells were starved overnight before reporter activities were measured (mean ± SD, $n = 6$, Student's *t*-test, n.s., not significant, $^{**}P < 0.01$, $^{***}P < 0.001$).

K, L FLAG-$HSF1^{WT}$ or FLAG-$HSF1^{S121A}$ plasmids were co-transfected with the dual HSF1 reporter plasmids into *HSF1*-deficient HEK293T cells for 2 days, followed by overnight starvation (mean ± SD, $n = 5$, Student's *t*-test, n.s., not significant, $^*P < 0.05$, $^{**}P < 0.01$).

Source data are available online for this figure.

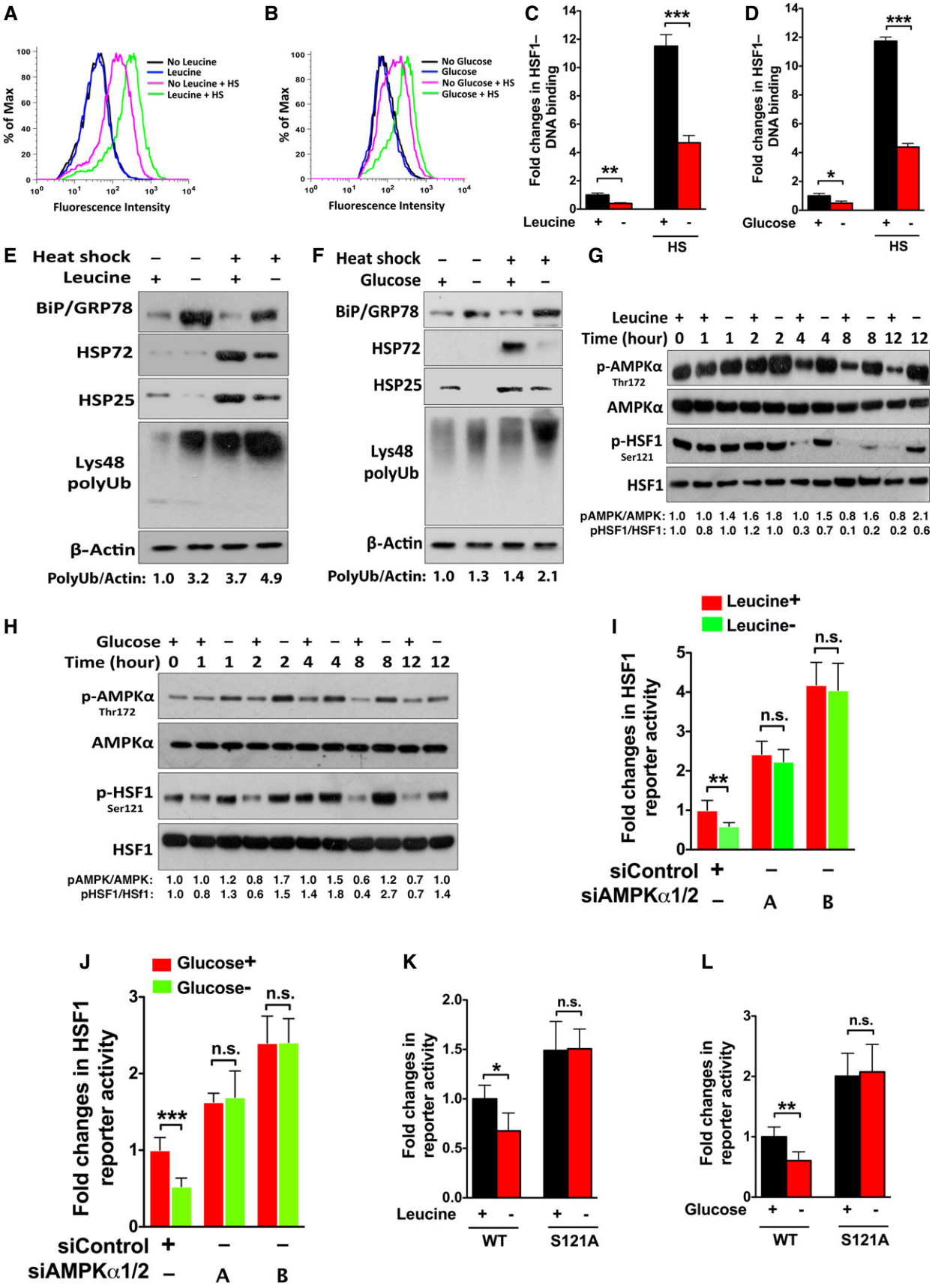
A
% of Max
Fluorescence Intensity
No Leucine
Leucine
No Leucine + HS
Leucine + HS
B
% of Max
Fluorescence Intensity
No Glucose
Glucose
No Glucose + HS
Glucose + HS
C
Fold changes in HSF1–DNA binding
Leucine
HS
D
Fold changes in HSF1–DNA binding
Glucose
HS
E
Heat shock
Leucine
BiP/GRP78
HSP72
HSP25
Lys48 polyUb
β-Actin
PolyUb/Actin: 1.0 3.2 3.7 4.9
F
Heat shock
Glucose
BiP/GRP78
HSP72
HSP25
Lys48 polyUb
β-Actin
PolyUb/Actin: 1.0 1.3 1.4 2.1
G
Leucine + + – + – + – + – + –
Time (hour) 0 1 1 2 2 4 4 8 8 12 12
p-AMPKα Thr172
AMPKα
p-HSF1 Ser121
HSF1
pAMPK/AMPK: 1.0 1.0 1.4 1.6 1.8 1.0 1.5 0.8 1.6 0.8 2.1
pHSF1/HSF1: 1.0 0.8 1.0 1.2 1.0 0.3 0.7 0.1 0.2 0.2 0.6
H
Glucose + + – + – + – + – + –
Time (hour) 0 1 1 2 2 4 4 8 8 12 12
p-AMPKα Thr172
AMPKα
p-HSF1 Ser121
HSF1
pAMPK/AMPK: 1.0 1.0 1.2 0.8 1.7 1.0 1.5 0.6 1.2 0.7 1.0
pHSF1/Hsf1: 1.0 0.8 1.3 0.6 1.5 1.4 1.8 0.4 2.7 0.7 1.4
I
Leucine+
Leucine-
Fold changes in HSF1 reporter activity
n.s.
siControl + – –
siAMPKα1/2 – A B
J
Glucose+
Glucose-
Fold changes in HSF1 reporter activity
n.s.
siControl + – –
siAMPKα1/2 – A B
K
Fold changes in reporter activity
n.s.
Leucine
WT
S121A
L
Fold changes in reporter activity
n.s.
Glucose
WT
S121A

Figure 4.

to enhanced nuclear translocation (Supplementary Fig S5D). Together, these results indicate that proteotoxic stress suppresses AMPK, which facilitates the PSR but impairs cellular responses to metabolic stressors. Intriguingly, metabolic and proteotoxic stressors exert opposite impacts on AMPK and HSF1 (Fig 5I).

Metabolic stressors disrupt proteostasis in tumor cells

Our and others' recent studies have pinpointed HSF1 as a potent facilitator of oncogenesis (Dai *et al*, 2007, 2012a; Min *et al*, 2007; Meng *et al*, 2010; Jin *et al*, 2011; Scott *et al*, 2011). In light of our new findings, we next asked whether HSF1 inactivation could contribute to the anti-neoplastic effects of metabolic stressors.

First, we examined the impact of 10 μM metformin, a clinically relevant concentration, on constitutive HSF1 activation in tumor cells. In WM115 and WM278 human melanoma cells, metformin impaired constitutive endogenous HSF1–DNA binding (Fig 6A) and diminished basal mRNA levels of *HSP72/HSPA1A* and *HSP27/HSPB1* (Fig 6B). Conversely, *AMPKα1/2* suppression not only elevated basal *HSP* expression but also antagonized metformin-mediated *HSP* suppression (Fig 6C and D). Compound C at 2 μM exerted similar effects, albeit to a lesser extent (Supplementary Fig S6A and B). To demonstrate HSP reduction at the protein level by metformin in tumor cells, prolonged treatment was applied to both block new synthesis of HSPs and deplete existing HSPs. Indeed, this prolonged treatment diminished HSP72 and HSP27 protein levels in a panel of diverse human tumor cell lines, ranging from melanoma (WM115 and A2058), to malignant peripheral nerve sheath tumor (MPNST) (S462), to colon carcinoma (RKO), and to breast adenocarcinoma (MCF-7 and MDA-MB-231) (Fig 6E; Supplementary Fig S6C–F).

Consistent with diminished HSP levels, metformin treatment elevated global protein Lys48 polyubiquitination in both detergent-soluble and detergent-insoluble fractions in diverse human tumor cell lines (Fig 6F and G; Supplementary Fig S6G–I). Importantly, co-treatment with compound C prevented HSP reduction, elevation of polyubiquitination, and increase in caspase 3 cleavage, which indicates apoptosis (Fig 6H). These results demonstrated a key role of AMPK in metformin-induced proteostasis disruption. Importantly, while *HSF1* knockdown reduced HSP expression and elevated protein polyubiquitination, treatment of *HSF1*-deficient cells with metformin failed to further induce polyubiquitination (Fig 6I), indicating that metformin disrupts proteostasis mainly through HSF1 suppression. Increased ubiquitination of detergent-insoluble proteins suggested aggravated protein aggregation (Fig 6F–I). To investigate this effect of metformin in detail, we developed a new method to measure intracellular protein aggregation. Our method is based on the Coulter principle, which detects the alterations in electrical impedance produced by particles suspended in an electrolyte (Zwicker, 2010), and which we adapted to quantitate the sizes of protein aggregates extracted from live cells. To use this method to quantitate protein aggregation, we measured aggregation of the GFP-tagged polyglutamine expansion tract (polyQ79) protein (Sanchez *et al*, 2003). Proteins with polyQ expansions are prone to misfolding and aggregation and are casually implicated in human neurodegenerative disorders (Muchowski & Wacker, 2005). While LacZ-expressing HEK293T cells contained only small aggregates that were barely detectable, polyQ79 expression markedly enlarged aggregates (Fig 6J), validating our new approach for aggregate quantitation. Importantly, both metformin and AMPKα^{CA} further enlarged these aggregates (Fig 6J), congruent with diminished HSP levels. Conversely, either HSF1 or a dominant negative AMPK mutant, AMPKα^{DN} (Mu *et al*, 2001), potently antagonized the enlargement of aggregates by metformin (Fig 6J), strongly suggesting a critical role of the AMPK–HSF1 pathway in metformin-induced protein aggregation. In further support of an aggravated protein aggregation, metformin caused a shift in distribution of polyQ proteins from detergent-soluble to detergent-insoluble fractions (Supplementary Fig S6J).

We previously demonstrated that HSF1 is essential to the growth and survival of tumor cells but dispensable for primary non-transformed cells (Dai *et al*, 2007). We reasoned that malignant cells might be more sensitive to metformin treatment than their non-transformed counterparts. To test this, we employed a pair of isogenic cell lines: immortalized MEFs and malignant derivatives of these cells that stably express oncogenic *HRAS*^{G12V}. In malignant MEFs, metformin impaired HSP72 expression, elevated protein polyubiquitination, and induced caspase 3 cleavage; in contrast, metformin had little effect on immortalized MEFs (Fig 6K). Interestingly, glucose deprivation exerted similar effects (Fig 6L) as well as aggravated polyQ aggregation (Fig 6M), all in a dose-dependent manner. Collectively, these results indicate that metabolic stressors suppress the HSF1-mediated PSR in malignant cells, thereby impairing their proteostasis and survival.

Figure 5. Heat shock suppresses AMPK and interferes with cellular responses to metabolic stressors.

A Reporter cells were heat-shocked at 43°C for the indicated time. AMPKα Thr172 and HSF1 Ser121 phosphorylation was measured by immunoblotting.

B Immediately following heat shock at 43°C for 40 min, AMPK complexes were immunoprecipitated from HEK293 cells and *in vitro* kinase assays were performed as described in Figure 3D using recombinant human ACC1 proteins as substrates.

C Following heat shock at 43°C for 40 min, both detergent-soluble and detergent-insoluble fractions of cellular proteins were extracted from HEK293 cells as described in Materials and Methods for immunoblotting.

D, E Immediately following heat shock at 43°C for 40 min, HEK293 cells were subjected to nutrient deprivations for 4 h. AMPKα Thr172 and ACC Ser79 phosphorylation was measured by immunoblotting.

F–H HSF1^{WT} or HSF1^{S121A} plasmids were transfected into *HSF1*-deficient HEK293T cells. Transfected cells were heat-shocked at 43°C for 40 min. *HSP* mRNAs were quantitated by qRT–PCR following overnight recovery. HSF1–DNA binding was measured immediately after heat shock (mean ± SD, $n = 3$, Student's *t*-test, $^{**}P < 0.01$, $^{***}P < 0.001$).

I Schematic depiction of the opposite impacts of metabolic and proteotoxic stress on AMPK and HSF1. While metabolic stress activates AMPK to suppress HSF1, proteotoxic stress suppresses AMPK to enhance HSF1 activation. Dashed arrow signifies HSF1 activation independent of AMPK.

Source data are available online for this figure.

Metformin inactivates HSF1 to retard tumor growth *in vivo*

Consistent with an HSF1 dependence of malignant cells, stable *HSF1* knockdown markedly impaired proliferation of A2058 and S462 cells (Fig 7A; Supplementary Fig S7A). This impairment was correlated with aggravated protein polyubiquitination (Fig 7B). In line with a role in HSF1 inactivation, the proliferation of A2058 and S462 cells was also impaired by metformin (Fig 7C; Supplementary

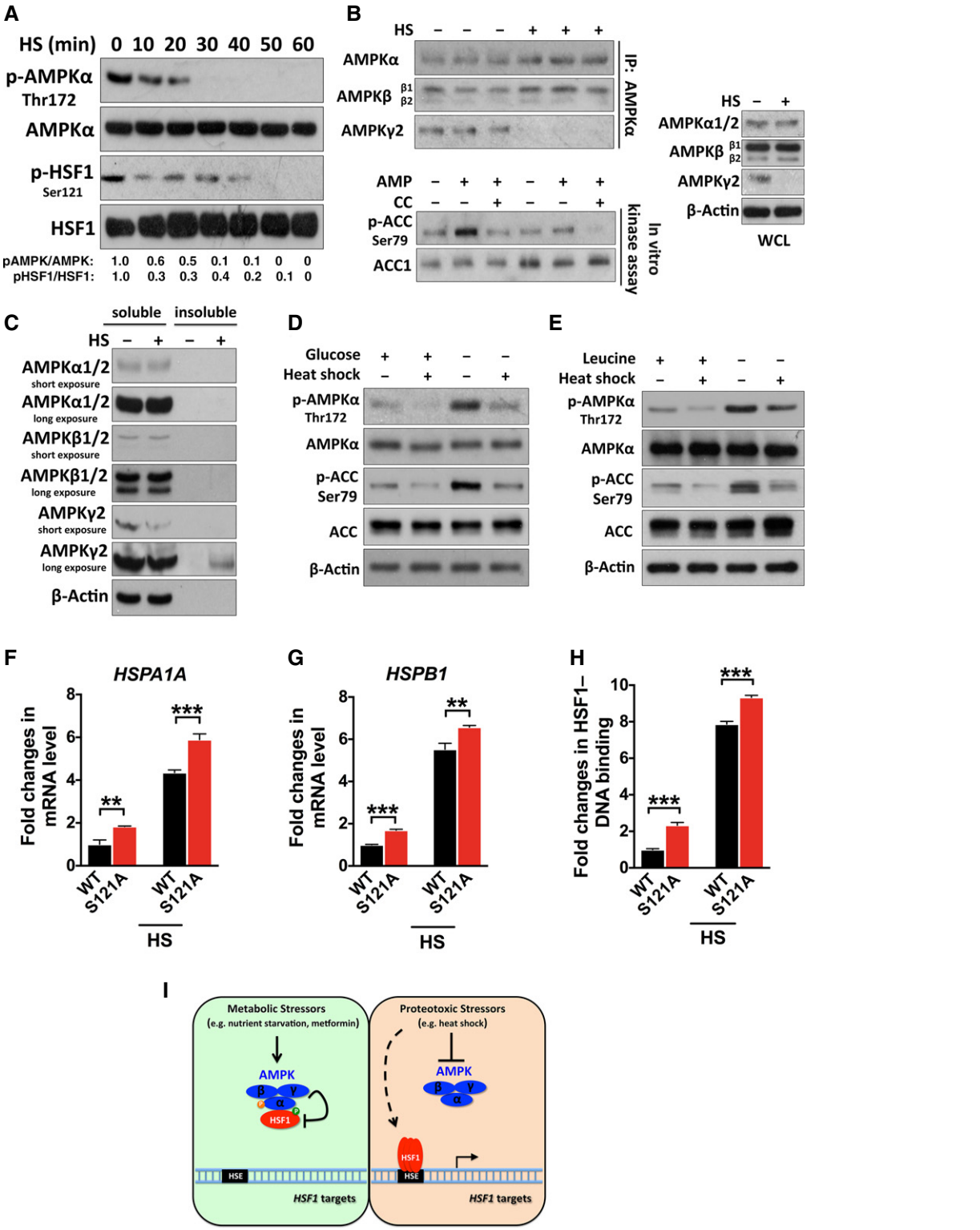

Figure 5.

Fig S7B). Of note, the anti-proliferation effect of metformin was more robust under low and normal glucose conditions than under high glucose conditions (Fig 7C; Supplementary Fig S7B), indicating a modifying effect of nutrients on metformin efficacy and consistent with a previous report (Javeshghani *et al*, 2012). Importantly, HSF1 overexpression significantly antagonized metformin-induced proliferation inhibition under normal and low glucose conditions (Fig 7C; Supplementary Fig S7B).

To examine the metformin–HSF1 interaction *in vivo*, we established a human melanoma xenograft model in NOD/SCID mice using A2058 cells that stably overexpressed either LacZ or HSF1. To provide clinical relevance, mice were administered metformin through drinking water at a concentration equivalent to the daily dose taken by T2D patients. Without metformin treatment, HSF1-expressing A2058 cells exhibited accelerated *in vivo* growth, evidenced by increased tumor incidence, volume, and mass, compared to LacZ-expressing cells (Fig 7D and E; Supplementary Fig S7C and D). Congruently, mice harboring HSF1-expressing cells exhibited shortened survival (Supplementary Fig S7E). These results demonstrate the pro-oncogenic role of HSF1. Congruent with its reported anti-neoplastic effects, metformin retarded the *in vivo* growth of both LacZ- and HSF1-expressing cells (Fig 7D and E; Supplementary Fig S7C and D). Importantly, HSF1-expressing tumors were less responsive to metformin treatment, indicated by less inhibited tumor incidence rate (30% vs. 58% inhibition in LacZ-expressing tumors; Supplementary Fig S7C), less prolonged tumor doubling time (32% vs. 61% prolongation in LacZ-expressing tumors; Fig 7E), and less reduced tumor mass (50% vs. 67% reduction in LacZ-expressing tumors; Supplementary Fig S7D). These results indicate partial metformin resistance engendered by HSF1. At the molecular level, metformin provoked proteotoxic stress, cell death, and AMPK activation in tumors, indicated by elevated protein polyubiquitination, caspase 3 cleavage, and AMPKα phosphorylation (Fig 7F). As expected, both AMPKα Thr172 and HSF1 Ser121 phosphorylation were elevated in metformin-treated tumors; interestingly, total HSF1 levels were also diminished by chronic metformin treatment (Fig 7F), congruent with HSF1 destabilization by metformin. Importantly, HSF1 overexpression not only potently antagonized these metformin-induced changes but also suppressed proteotoxic stress and cell death under basal conditions (Fig 7F). In sharp contrast, metformin did not provoke proteotoxic stress and cell death in normal mouse livers (Fig 7G; Supplementary Fig S7F), demonstrating a distinct sensitivity of tumor tissues to metformin. Given that chronic metformin treatment induced both Ser121 phosphorylation and depletion of HSF1 in tumors, we further investigated the importance of Ser121 phosphorylation in metformin-mediated anti-neoplastic effects. To address this, we generated a pair of isogenic A2058 cell lines, in which endogenous HSF1 was substituted with either FLAG-HSF1^{WT} or FLAG-HSF1^{S121A}. These engineered cell lines expressed comparable levels of HSF1 (Supplementary Fig S7G). Whereas metformin markedly suppressed HSP expression and induced protein ubiquitination in HSF1^{WT}-expressing cells, these effects were largely abolished in HSF1^{S121A}-expressing cells (Fig 7H). In consequence, the proliferation of HSF1^{S121A}-expressing cells was less impaired by metformin compared to that of HSF1^{WT}-expressing cells under adherent conditions (Supplementary Fig S7H). Moreover, HSF1^{S121A}-expressing cells were also more resistant to metformin treatment under anchorage-independent growth conditions. This was demonstrated in both suspension cultures and soft agar assays (Fig 7I and Supplementary Fig S7I). While in suspension cultures, cells expressing HSF1^{WT} were sensitive to metformin at all glucose concentrations, they only responded to metformin at normal and low glucose concentrations in soft agar (Supplementary Fig S7I). Of note, glucose concentrations had a marked impact on cellular growth in soft agar. In low-glucose medium, the growth of both HSF1^{S121A}- and HSF1^{WT}-expressing cells was severely impaired (Supplementary Fig S7I). Nonetheless, a slight metformin resistance was still observed in HSF1^{S121A}-expressing cells (Supplementary Fig S7I). We reasoned that such stringent growth conditions might alleviate cellular dependence on HSF1, which is distinct from suspension growth conditions (Fig 7I). These results together suggest that HSF1 Ser121 phosphorylation plays an important role in metformin-mediated anti-neoplastic effects.

Evidence from human patients also supported the AMPK-HSF1 interaction. In a large-cohort study of patients developing clear cell renal cell carcinomas (ccRCC) (Cancer Genome Atlas Research Network, 2013), tumors showing elevated AMPKα Thr172 phosphorylation displayed reduced mRNA levels of *HSPA1A*, *HSPA1B*,

Figure 6. Metabolic stressors inactivate HSF1 and disrupt proteostasis in tumor cells.

A, B Following treatment with 10 μM metformin for 3 days, the levels of HSF1 binding to endogenous *HSP* promoters were quantitated by chromatin IP (mean ± SD, $n = 3$, one-way ANOVA, $^{**}P < 0.01$, $^{***}P < 0.001$). Normal rabbit IgG served as the negative control (A). Following the same treatment, *HSP* mRNA levels were quantitated by qRT–PCR (mean ± SD, $n = 3$, Student's *t*-test, $^{***}P < 0.001$) (B).

C, D Following transfection with *AMPKα1/2*-targeting siRNAs for 2 days, WM115 cells were treated with 10 μM metformin for 3 days. *HSP* mRNA levels were quantitated by qRT–PCR (mean ± SD, $n = 6$, Student's *t*-test, n.s., not significant, $^{*}P < 0.05$, $^{**}P < 0.01$).

E Following treatment with 10 μM metformin for 7 days, protein levels in WM115 and S462 cells were measured by immunoblotting.

F, G Following treatment with 10 μM metformin for 7 days, levels of polyubiquitinated proteins were detected in both detergent-soluble and detergent-insoluble fractions in WM115 and A2058 cells using a Lys48-specific polyubiquitin antibody.

H A2058 cells were treated with 10 μM metformin alone or co-treated with 2 μM compound C for 7 days. Individual proteins were detected by immunoblotting.

I HEK293T cells stably expressing either scramble or *HSF1*-targeting shRNAs were treated with 10 μM metformin for 7 days. Individual proteins were detected by immunoblotting.

J In HEK293T cells, a plasmid encoding HA-polyQ79-GFP was co-transfected with the indicated plasmids. Following treatment with and without 10 μM metformin for 5 days, the sizes of aggregates in detergent-insoluble fractions were quantitated by a Multisizer™ 3 Coulter Counter. Experimental details are described in Materials and Methods.

K, L Immortalized and *RAS*-transformed MEFs were treated with either 10 μM metformin (K) or different concentrations of glucose (L) for 7 days. Individual proteins were detected by immunoblotting.

M Following transfection with LacZ or polyQ79, HEK293T cells were grown under different concentrations of glucose for 5 days before measuring aggregate size.

Source data are available online for this figure.

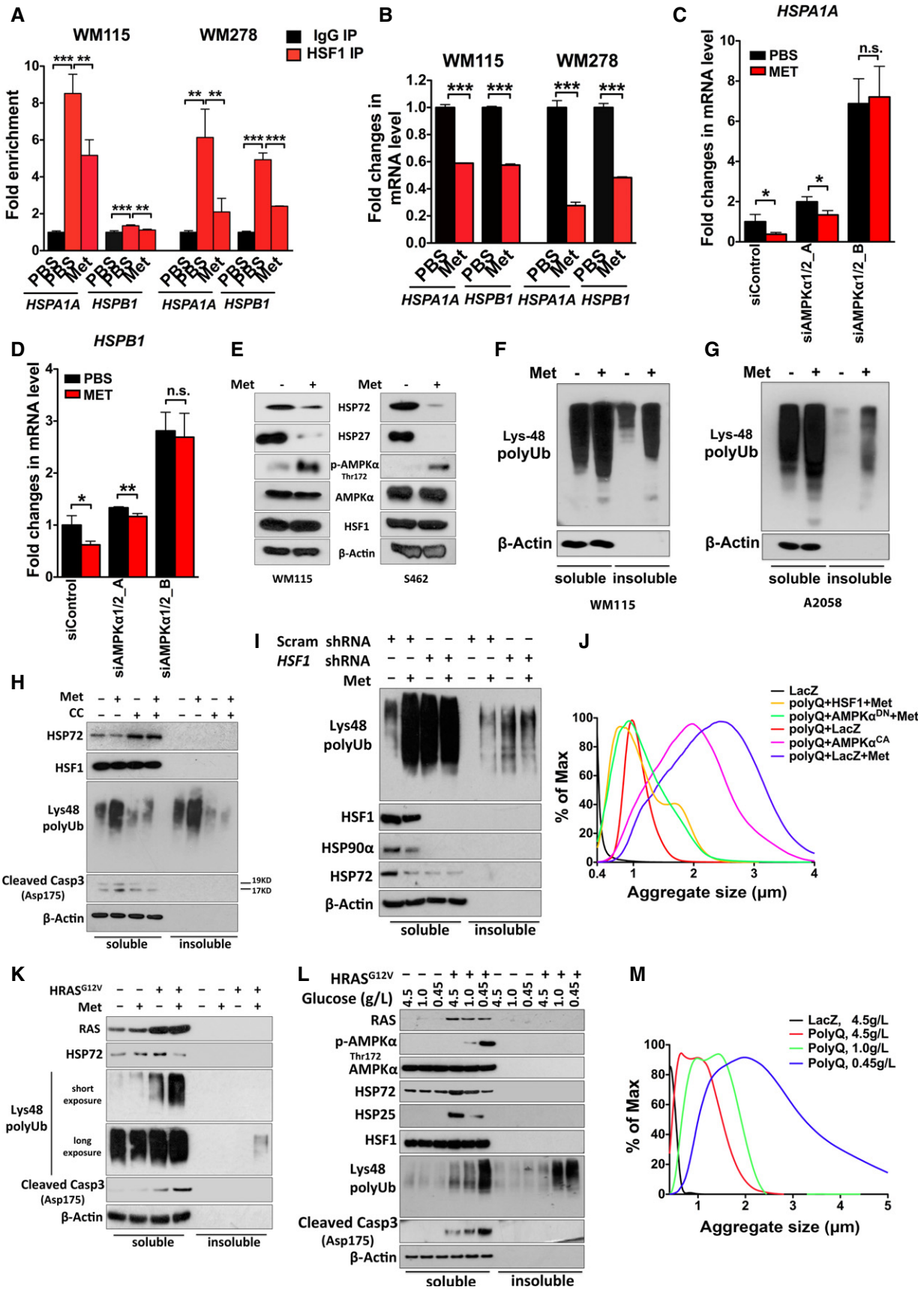
A
WM115
WM278
IgG IP
HSF1 IP
Fold enrichment
PBS
Met
HSPA1A
HSPB1
B
Fold changes in mRNA level
C
HSPA1A
PBS
MET
n.s.
siControl
siAMPKα1/2_A
siAMPKα1/2_B
D
HSPB1
E
HSP72
HSP27
p-AMPKα
Thr172
AMPKα
HSF1
β-Actin
WM115
S462
F
Lys-48 polyUb
soluble
insoluble
G
A2058
H
Cleaved Casp3 (Asp175)
19KD
17KD
I
Scram shRNA
HSF1 shRNA
HSP90α
J
LacZ
polyQ+HSF1+Met
polyQ+AMPKα^DN+Met
polyQ+LacZ
polyQ+AMPKα^CA
polyQ+LacZ+Met
% of Max
Aggregate size (μm)
K
HRAS^G12V
RAS
short exposure
long exposure
L
Glucose (g/L)
M
LacZ, 4.5g/L
PolyQ, 4.5g/L
PolyQ, 1.0g/L
PolyQ, 0.45g/L

Figure 6.

HSPB1, and *HSP90AA1*, all of which are classic HSF1 transcriptional targets (Fig 7J), suggesting inhibition of HSF1. Moreover, ccRCC patients with high levels of AMPKα phosphorylation demonstrated better overall survival (Supplementary Fig S7J; Cancer Genome Atlas Research Network, 2013). Taken together, these results indicate that a clinically relevant concentration of metformin suppresses constitutive HSF1 activation and disrupts proteostasis within tumor cells, thereby retarding tumor growth (Fig 7K).

Discussion

Our findings unveil a novel interplay between AMPK and HSF1. AMPK inactivates HSF1 through phosphorylation of it at Ser121. This regulation, remarkably, impacts stress resistance, proteostasis, and malignant growth.

HSF1 at the crossroads of the metabolic and proteotoxic stress responses

In response to fluctuations of intracellular AMP and ATP levels, AMPK critically preserves energy homeostasis by stimulating ATP production and suppressing ATP consumption (Hardie, 2011). This metabolic switch driven by AMPK enables cells to survive energy stress. To survive and adapt to such stress, it is imperative for cells to downscale anabolic processes such as lipid and protein production. Metabolic stress activates AMPK, which subsequently inhibits activities of SREBP1 and mTORC1 (Gwinn *et al*, 2008; Li *et al*, 2011), key regulators of lipid and protein synthesis. Significantly, our findings indicate that AMPK likely plays an additional key role in survival of metabolic stress. Similar to the case with lipid and protein synthesis, processes involved with chaperone-mediated protein folding and anti-aggregation also consume ATP (Welch, 1991). It becomes wasteful energetically to sustain excessive chaperoning capacity when overall protein synthesis is mitigated, as is the case during times of stress. Therefore, it is a logical action of cells to diminish chaperone production, through inactivation of HSF1, in the face of metabolic stress. Thus, our findings expand the roles of AMPK in protein metabolism beyond mTORC1-mediated translational control and reveal that by gauging cellular energy status, AMPK finely orchestrates protein quantity and quality control machineries. In this sense, our findings suggest attenuation of the PSR as an integral part of the cellular adaption to metabolic stress.

Inactivation of HSF1 by amino acid starvation was reported previously (Hensen *et al*, 2012), although the underlying mechanisms remained elusive. Now, our findings reveal that the metabolic and proteotoxic stress responses, two fundamental cellular stress pathways, are interconnected through AMPK and HSF1. Whereas metabolic stressors activate AMPK but suppress HSF1, our results reveal that proteotoxic stressors, such as heat shock, exert the opposite effects at least in the cell types we examined (Fig 5I). Although the response to each individual stress is advantageous to survival of that stress, this antagonizing interaction between the two responses could have adverse impacts in the face of simultaneous exposure to the two stresses (Figs 4E and F, and 5D and E). While our results indicate diminished AMPK activities under heat shock in NIH3T3 and HEK293 cells (Fig 5A–C; Supplementary Fig S5A), it was previously reported that heat shock activated AMPK in rat hepatocytes (Corton *et al*, 1994), a highly metabolically active cell type. Thus, these results suggest that AMPK response to heat stress may be cell type dependent.

Implications of AMPK–HSF1 interactions in human diseases and therapies

Evidence is emerging that implicates AMPK in neurodegeneration. Neuronal AMPK activation has been noted in Huntington's disease and Alzheimer's disease and contributes to neuronal death (Ju *et al*, 2011; Vingtdeux *et al*, 2011). Thus, it is tantalizing to speculate that AMPK activation may aggravate neurodegeneration in part through impairment of neuronal proteostasis. Exacerbation of polyQ aggregation inflicted by metformin, glucose deprivation, or activated AMPK (Fig 6J and M) supports this possibility. Further, our findings imply a potential adverse side effect of metformin on populations afflicted with neurodegenerative disorders, a notion that may deserve further investigation.

Figure 7. Metformin inactivates HSF1 to retard tumor growth.

A, B A2058 cells were transduced with lentiviral scramble or *HSF1*-targeting (hA6 and hA9) shRNAs. (A) Cell numbers were quantitated by Hoechst 33342 DNA staining (mean ± SD, $n = 4$, two-way ANOVA, $^{***}P < 0.001$). (B) Protein levels were measured by immunoblotting.

C A2058 cells stably expressing LacZ or HSF1 were grown in medium containing 4.5, 1.0, or 0.45 g/l glucose. Following treatment with 10 μM metformin, cell proliferation was measured by Hoechst 33342 DNA staining (mean ± SD, $n = 5$, two-way ANOVA, $^{***}P < 0.001$).

D, E 1×10^6 LacZ- or HSF1-expressing A2058 cells were transplanted into female NOD/SCID mice. One day after transplantation, metformin was administered via drinking water at 1 mg/ml. Tumor incidence (log-rank test; D) and volumes (E) were measured (mean ± SEM, two-way ANOVA n.s., not significant, $^{*}P < 0.05$, $^{**}P < 0.01$, $^{***}P < 0.001$). Tumor growth curves were fitted to exponential growth models to calculate tumor doubling time (DT).

F Individual proteins were measured by immunoblotting using lysates of three tumors from each treatment group.

G Protein levels were measured by immunoblotting using lysates of mouse liver tissues.

H A2058 cells stably expressing FLAG-HSF1^{WT} or FLAG-HSF1^{S121A} were treated with 10 μM metformin for 7 days. Protein levels were measured by immunoblotting.

I A2058 cells stably expressing HSF1^{WT} or HSF1^{S121A} were grown in Corning®ultra-low attachment 96-well culture plates with 10 μM metformin and different concentrations of glucose for 7 days, 10,000 cells per well. Viable cells were counted by Guava flow cytometer using ViaCount® reagent (mean ± SEM, $n = 8$, Student's *t*-test, n.s., not significant, $^{**}P < 0.01$, $^{***}P < 0.001$).

J Tukey box plots showing the inverse correlation between AMPKα Thr172 phosphorylation and *HSP* mRNA expression in ccRCC. Patients were stratified on the median value of AMPKα Thr172 phosphorylation reverse-phase protein array (RPPA) scores (Student's *t*-test).

K Schematic depiction of the suppression of HSF1 and disruption of proteostasis by AMPK in malignant transformation.

Source data are available online for this figure.

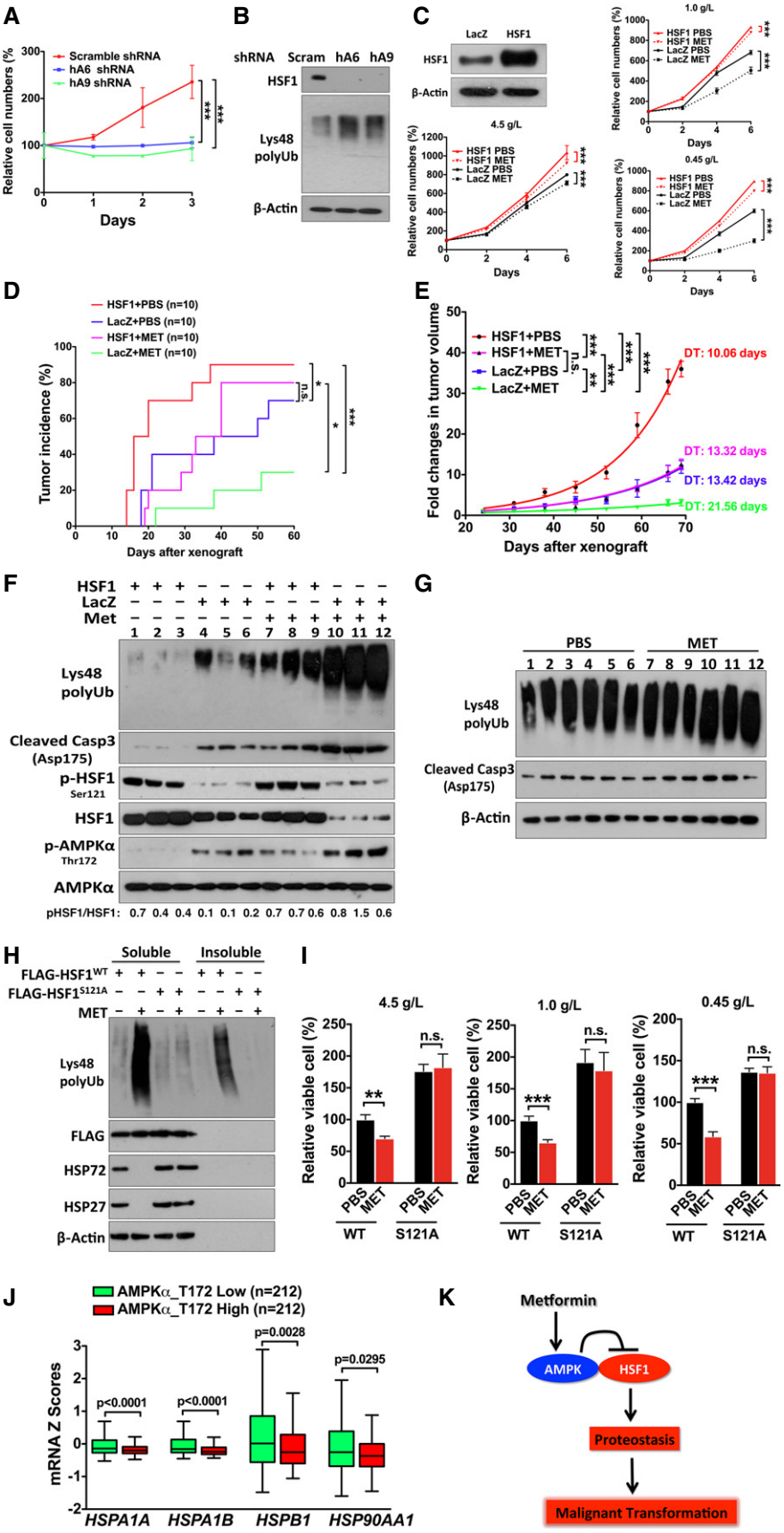

Figure 7.

Despite the importance of the HSF1-mediated PSR in oncogenesis, it remains poorly understood how malignant cells hijack this powerful adaptive mechanism. The negative regulation of HSF1 by AMPK, thus, may shed new light on this question. Previous studies have demonstrated many anti-neoplastic effects of the LKB1–AMPK pathway. LKB1 functions as a tumor suppressor and its germline mutations are causally linked to Peutz–Jeghers syndrome (Shackelford & Shaw, 2009). In addition, AMPK stimulates tumor suppressors including TSC2 and TP53 (Inoki *et al*, 2003; Jones *et al*, 2005), and its inactivation promotes oncogenesis (Faubert *et al*, 2013). Now our findings reveal an important role of the tumor-suppressive AMPK pathway in inactivating HSF1. Conceivably, inactivation of the LKB1–AMPK pathway could in a cell-autonomous fashion mobilize the PSR to assist malignant transformation. This resonates with the interaction between HSF1 and the tumor suppressor NF1 we discovered recently, in which *NF1* deficiency sufficiently activates HSF1 to promote oncogenesis (Dai *et al*, 2012a). These negative regulations of HSF1 mediated by tumor-suppressive pathways highlight the notion that activation of HSF1 and its mediated PSR is deeply embedded within oncogenic processes.

Our findings also uncover a novel mechanism of action of metformin. The principal metabolic effects of metformin result from suppressed liver gluconeogenesis and enhanced muscle glucose uptake (Viollet *et al*, 2012). In addition to these well-known anti-diabetic benefits, epidemiological studies have revealed reduced tumor incidence in T2D patients taking metformin (Evans *et al*, 2005; Garrett *et al*, 2012; Sadeghi *et al*, 2012). Preclinical investigations show that metformin impaired *de novo* oncogenesis in mice and impeded tumor growth in xenograft models (Anisimov *et al*, 2010; Memmott *et al*, 2010; Iliopoulos *et al*, 2011; Tomic *et al*, 2011). Despite this exciting promise, the proposed underlying mechanisms are diverse, ranging from reduced insulin levels, to suppressed mTORC1 activity, to activated TP53, and to impaired NF-κB signaling (Buzzai *et al*, 2007; Dowling *et al*, 2007; Hirsch *et al*, 2013).

Now our findings indicate that metformin suppresses the HSF1-mediated PSR. Importantly, due to the lack of proteotoxic stress, HSF1 is dispensable for the viability of primary cells and mice under non-stress conditions (Xiao *et al*, 1999; Dai *et al*, 2007). In stark contrast, malignant cells constantly endure proteotoxic stress from within and without and, in turn, develop an addiction to HSF1 to sustain their robustness (Dai *et al*, 2007, 2012b). Congruently, whereas in malignant cells a clinically relevant concentration of metformin and mild glucose deprivation suppressed constitutive HSF1 activation, aggravating proteomic imbalance and impairing survival, little impact was observed in non-transformed cells (Figs 6K and L, and 7F and G), indicating a promising therapeutic window. Moreover, our results showing partial resistance of tumors to metformin as a result of HSF1 expression (Fig 7D–F) highlight the importance of this specific mechanism to metformin's overall anti-neoplastic effects and further imply that tumors with low levels of HSF1 expression may be more sensitive to metformin treatment. Our findings collectively suggest a novel unifying mechanism of action of metabolic stressors in malignancy—disruption of proteostasis via HSF1 inactivation.

Materials and Methods

An ELISA-based HSF1–DNA binding assay

Biotinylated ideal HSE (CTAGAAGCTTCTAGAAGCTTCTAG) oligonucleotides were self-annealed to form double-stranded DNA probes in annealing buffer (10 mM Tris, pH 7.5, 50 mM NaCl, 1 mM EDTA). To immobilize these probes for HSF1 binding, 100 μl of 500 nM biotinylated HSE probes diluted in PBS was added to neutravidin-coated 96-well plates (Thermo Scientific) and incubated at 4°C overnight. After washing with PBS once, wells were incubated with 200 μl SuperBlock blocking buffer (Thermo Scientific) at RT for 1 h. After washing with 1× DNA binding buffer (10 mM Tris, 50 mM NaCl, 1 mM EDTA, 5% glycerol, pH 7.5) once, 100 μl nuclear proteins diluted in 1× DNA binding buffer was added to each well and incubated at RT for 40 min. The captured protein–DNA binding was stabilized by immediately incubating the wells with 1% formaldehyde diluted in 1× DNA binding buffer at RT for 5 min. Following washing 3 times with 1× DNA binding buffer, each well was incubated with 100 μl rabbit polyclonal HSF1 antibody (B7109, Assay Biotechnology) diluted 1:1,000 in SuperBlock blocking buffer at RT for 2 h. After TBS-T washing, each well was incubated with HRP-conjugated anti-rabbit IgG secondary antibodies diluted in the blocking buffer at RT for 1 h. Following extensive TBS-washing, colorimetric signals were developed using 1-Step Ultra TMB-ELISA substrate (Thermo Scientific).

To validate this method, nuclear extracts of heat-shocked $Hsf1^{+/+}$ and $Hsf1^{-/-}$ cells were used to serve as positive and negative controls, respectively. Assay specificity was further validated by pre-incubating nuclear extracts with non-biotinlyated ideal HSE or a scramble oligonucleotide of the HSE (GCGACATTATTGGTGCAACATTAC).

Bioluminescence imaging

Transgenic Hsp70-luc-2A-eGFP reporter mice (FVB/NJ/C57BL/6J background) were obtained from The Jackson Laboratory. Mice of the same sex at 5–6 weeks of age were treated with metformin for 3 days via i.p. injection. Six hours before bioluminescence imaging, mice were challenged with a single dose of velcade via i.p. injection. Before imaging, XenoLight RediJect D-luciferin (150 mg/kg) was i.p. injected into mice. Mice were anesthetized with isoflurane, and luminescence signals were recorded using a Xenogen IVIS Lumina II system (Caliper Life Sciences). Images of both dorsal and ventral positions were captured. The total photon flux of each mouse was quantified using Living Image software.

Proximity ligation assay

Following treatments, cells were fixed with 4% formaldehyde in PBS for 15 min at RT. After blocking with 5% normal goat serum in PBS with 0.3% Triton X-100, a pair of rabbit and mouse primary antibodies were incubated simultaneously with fixed cells. To detect HSF1–DNA interactions, fixed cells were treated with 7 U/ml RNase at RT for 1 h before incubation with rabbit anti-HSF1 antibodies (H-311, Santa Cruz Biotechnology) and mouse monoclonal anti-ds DNA antibody (HYB331-01, Santa

Cruz Biotechnology) overnight at 4°C. To detect phospho-AMPKα–HSF1 interactions, fixed cells were incubated with rabbit monoclonal phospho-AMPKα Thr172 antibodies (40H9, Cell Signal Technology) and mouse monoclonal HSF1 antibodies (E-4, Santa Cruz Biotechnology) overnight at 4°C. All primary antibodies were used at 1:50 dilution in blocking buffer. Following incubation with Duolink PLA anti-rabbit Plus and anti-mouse Minus probes (OLINK Bioscience) at 37°C for 1 h, ligation, rolling circle amplification, and detection were performed using the Duolink In Situ Detection Reagents Red (OLINK Bioscience) as per manufacturer's instructions. Nuclei were counterstained with Hoechst 33342. Finally, PLA signals were documented by a Leica TCS SP5 confocal microscope.

Soluble and insoluble protein fractionation

Equal numbers of cells were incubated with cell lysis buffer containing 1% Triton X-100 on ice for 20 min. The crude lysates were first centrifuged at 500 *g* for 2 min at 4°C. The supernatants were further centrifuged at 20,000 *g* for 20 min at 4°C. The final supernatants and pellets were collected as detergent-soluble and detergent-insoluble fractions, respectively. Insoluble fractions were further subjected to sonication for SDS–PAGE.

Measurement of aggregate size

Equal numbers of cells from different samples were lysed with cold cell lysis buffer. Following centrifugation at 20,000 *g* for 15 min at 4°C, detergent-insoluble pellets were further extracted with RIPA buffer 3 times. The final insoluble pellets were re-suspended in 10% SDS by pipetting and immediately subjected to aggregate sizing using a Multisizer™ 3 Coulter Counter equipped with a 20-μm aperture (Beckman Coulter).

Animal studies

Ampkα1$^{fl/fl}$ and *Ampkα2*$^{fl/fl}$ mutant mice on the C57BL/6J background were obtained from The Jackson Laboratory. *Hsf1* mutant mice (129SvJ/BALB/cJ) were a generous gift from Dr. Ivor Benjamin (Xiao *et al*, 1999) and described previously (Dai *et al*, 2007, 2012b).

For tumor xenograft studies, 1×10^6 A2058 cells were s.c. injected into the left flanks of 9-week-old female NOD.CB17-Prkdc<scid>/J (NOD/SCID) mice (The Jackson Laboratory). One day after injection, mice were given 1 mg/ml metformin via water held in light-tight drinking bottles. This dose is calculated based on 1,000 mg/60 kg/day in humans. The equivalent mouse dose is 205 mg/kg/day, which corresponds to about 4 mg/day for a 20 g adult mouse consuming 4 ml water per day. Tumor sizes were measured by a caliper weekly, and tumor volumes were calculated following the formula $4/3\pi R^3$. All mouse experiments were performed under a protocol approved by The Jackson Laboratory Animal Care and Use Committee.

Statistical methods

All statistical analyses were performed using Prism 5.0 (GraphPad software). Statistical significance: $^*P < 0.05$; $^{**}P < 0.01$; $^{***}P < 0.001$.

Supplementary information for this article is available online: http://emboj.embopress.org

Acknowledgements

We would like to thank Dr. Ivor Benjamin for *Hsf1* MEFs and mice; Dr. Luke Whitesell for cell lines; Barbara Tennent for critically reading the manuscript; and Xin Wang and Xiongtao Ruan for their technical assistance. This work was supported in part by The Jackson Laboratory Cancer Center Support Grant (3P30CA034196), and grants from NIH (1DP2OD007070) and the Ellison Medical Foundation (AS-NS-0599-09) to C.D.

Author contributions

SD performed immunoblotting, bioluminescence imaging, flow cytometry experiments, body weight composition analysis, and *in vivo* shRNA delivery; ZT performed DNA binding, ChIP, and immunoblotting experiments; JC and WZ performed immunoprecipitation, PLA, and measurement of aggregate size experiments; HL performed cell growth and viability experiments; CD conceived the project and oversaw the studies; SS and CD wrote the manuscript.

Conflict of interest

The authors declare that they have no conflict of interest.

References

Anisimov VN, Egormin PA, Piskunova TS, Popovich IG, Tyndyk ML, Yurova MN, Zabezhinski MA, Anikin IV, Karkach AS, Romanyukha AA (2010) Metformin extends life span of HER-2/neu transgenic mice and in combination with melatonin inhibits growth of transplantable tumors in vivo. *Cell Cycle* 9: 188 – 197

Balch WE, Morimoto RI, Dillin A, Kelly JW (2008) Adapting proteostasis for disease intervention. *Science* 319: 916 – 919

Blair E, Redwood C, Ashrafian H, Oliveira M, Broxholme J, Kerr B, Salmon A, Ostman-Smith I, Watkins H (2001) Mutations in the gamma (2)-subunit of AMP-activated protein kinase cause familial hypertrophic cardiomyopathy: evidence for the central role of energy compromise in disease pathogenesis. *Hum Mol Genet* 10: 1215 – 1220

Buzzai M, Jones RG, Amaravadi RK, Lum JJ, DeBerardinis RJ, Zhao F, Viollet B, Thompson CB (2007) Systemic treatment with the antidiabetic drug metformin selectively impairs p53-deficient tumor cell growth. *Cancer Res* 67: 6745 – 6752

Cancer Genome Atlas Research Network (2013) Comprehensive molecular characterization of clear cell renal cell carcinoma. *Nature* 499: 43 – 49

Chou SD, Prince T, Gong J, Calderwood SK (2012) mTOR is essential for the proteotoxic stress response, HSF1 activation and heat shock protein synthesis. *PLoS ONE* 7: e39679

Clausson CM, Allalou A, Weibrecht I, Mahmoudi S, Farnebo M, Landegren U, Wahlby C, Soderberg O (2011) Increasing the dynamic range of in situ PLA. *Nat Methods* 8: 892 – 893

Corton JM, Gillespie JG, Hardie DG (1994) Role of the AMP-activated protein kinase in the cellular stress response. *Curr Biol* 4: 315 – 324

Corton JM, Gillespie JG, Hawley SA, Hardie DG (1995) 5-aminoimidazole-4-carboxamide ribonucleoside. A specific method for activating AMP-activated protein kinase in intact cells? *Eur J Biochem* 229: 558 – 565

Dai C, Whitesell L, Rogers AB, Lindquist S (2007) Heat shock factor 1 is a powerful multifaceted modifier of carcinogenesis. *Cell* 130: 1005 – 1018

Dai C, Santagata S, Tang Z, Shi J, Cao J, Kwon H, Bronson RT, Whitesell L, Lindquist S (2012a) Loss of tumor suppressor NF1 activates HSF1 to promote carcinogenesis. *J Clin Invest* 122: 3742 – 3754

Dai C, Dai S, Cao J (2012b) Proteotoxic stress of cancer: implication of the heat-shock response in oncogenesis. *J Cell Physiol* 227: 2982 – 2987

Dowling RJ, Zakikhani M, Fantus IG, Pollak M, Sonenberg N (2007) Metformin inhibits mammalian target of rapamycin-dependent translation initiation in breast cancer cells. *Cancer Res* 67: 10804 – 10812

Dowling RJ, Goodwin PJ, Stambolic V (2011) Understanding the benefit of metformin use in cancer treatment. *BMC Med* 9: 33

Dowling RJ, Niraula S, Stambolic V, Goodwin PJ (2012) Metformin in cancer: translational challenges. *J Mol Endocrinol* 48: R31 – R43

Egan DF, Shackelford DB, Mihaylova MM, Gelino S, Kohnz RA, Mair W, Vasquez DS, Joshi A, Gwinn DM, Taylor R, Asara JM, Fitzpatrick J, Dillin A, Viollet B, Kundu M, Hansen M, Shaw RJ (2011) Phosphorylation of ULK1 (hATG1) by AMP-activated protein kinase connects energy sensing to mitophagy. *Science* 331: 456 – 461

El-Mir MY, Nogueira V, Fontaine E, Averet N, Rigoulet M, Leverve X (2000) Dimethylbiguanide inhibits cell respiration via an indirect effect targeted on the respiratory chain complex I. *J Biol Chem* 275: 223 – 228

Evans JM, Donnelly LA, Emslie-Smith AM, Alessi DR, Morris AD (2005) Metformin and reduced risk of cancer in diabetic patients. *BMJ* 330: 1304 – 1305

Faubert B, Boily G, Izreig S, Griss T, Samborska B, Dong Z, Dupuy F, Chambers C, Fuerth BJ, Viollet B, Mamer OA, Avizonis D, DeBerardinis RJ, Siegel PM, Jones RG (2013) AMPK is a negative regulator of the Warburg effect and suppresses tumor growth in vivo. *Cell Metab* 17: 113 – 124

Garrett CR, Hassabo HM, Bhadkamkar NA, Wen S, Baladandayuthapani V, Kee BK, Eng C, Hassan MM (2012) Survival advantage observed with the use of metformin in patients with type II diabetes and colorectal cancer. *Br J Cancer* 106: 1374 – 1378

Göransson O, McBride A, Hawley SA, Ross FA, Shpiro N, Foretz M, Viollet B, Hardie DG, Sakamoto K (2007) Mechanism of action of A-769662, a valuable tool for activation of AMP-activated protein kinase. *J Biol Chem* 282: 32549 – 32560

Gwinn DM, Shackelford DB, Egan DF, Mihaylova MM, Mery A, Vasquez DS, Turk BE, Shaw RJ (2008) AMPK phosphorylation of raptor mediates a metabolic checkpoint. *Mol Cell* 30: 214 – 226

Hardie DG (2011) AMP-activated protein kinase: an energy sensor that regulates all aspects of cell function. *Genes Dev* 25: 1895 – 1908

Hawley SA, Davison M, Woods A, Davies SP, Beri RK, Carling D, Hardie DG (1996) Characterization of the AMP-activated protein kinase kinase from rat liver and identification of threonine 172 as the major site at which it phosphorylates AMP-activated protein kinase. *J Biol Chem* 271: 27879 – 27887

Hensen SM, Heldens L, van Enckevort CM, van Genesen ST, Pruijn GJ, Lubsen NH (2012) Heat shock factor 1 is inactivated by amino acid deprivation. *Cell Stress Chaperones* 17: 743 – 755

Hirsch HA, Iliopoulos D, Struhl K (2013) Metformin inhibits the inflammatory response associated with cellular transformation and cancer stem cell growth. *Proc Natl Acad Sci USA* 110: 972 – 977

Hsu AL, Murphy CT, Kenyon C (2003) Regulation of aging and age-related disease by DAF-16 and heat-shock factor. *Science* 300: 1142 – 1145

Iliopoulos D, Hirsch HA, Struhl K (2011) Metformin decreases the dose of chemotherapy for prolonging tumor remission in mouse xenografts involving multiple cancer cell types. *Cancer Res* 71: 3196 – 3201

Inoki K, Zhu T, Guan KL (2003) TSC2 mediates cellular energy response to control cell growth and survival. *Cell* 115: 577 – 590

Javeshghani S, Zakikhani M, Austin S, Bazile M, Blouin MJ, Topisirovic I, St-Pierre J, Pollak MN (2012) Carbon source and myc expression influence the antiproliferative actions of metformin. *Cancer Res* 72: 6257 – 6267

Jin X, Moskophidis D, Mivechi NF (2011) Heat shock transcription factor 1 is a key determinant of HCC development by regulating hepatic steatosis and metabolic syndrome. *Cell Metab* 14: 91 – 103

Jones RG, Plas DR, Kubek S, Buzzai M, Mu J, Xu Y, Birnbaum MJ, Thompson CB (2005) AMP-activated protein kinase induces a p53-dependent metabolic checkpoint. *Mol Cell* 18: 283 – 293

Ju TC, Chen HM, Lin JT, Chang CP, Chang WC, Kang JJ, Sun CP, Tao MH, Tu PH, Chang C, Dickson DW, Chern Y (2011) Nuclear translocation of AMPK-alpha1 potentiates striatal neurodegeneration in Huntington's disease. *J Cell Biol* 194: 209 – 227

Kahn BB, Alquier T, Carling D, Hardie DG (2005) AMP-activated protein kinase: ancient energy gauge provides clues to modern understanding of metabolism. *Cell Metab* 1: 15 – 25

Kalender A, Selvaraj A, Kim SY, Gulati P, Brule S, Viollet B, Kemp BE, Bardeesy N, Dennis P, Schlager JJ, Marette A, Kozma SC, Thomas G (2010) Metformin, independent of AMPK, inhibits mTORC1 in a rag GTPase-dependent manner. *Cell Metab* 11: 390 – 401

Kondo N, Katsuno M, Adachi H, Minamiyama M, Doi H, Matsumoto S, Miyazaki Y, Iida M, Tohnai G, Nakatsuji H, Ishigaki S, Fujioka Y, Watanabe H, Tanaka F, Nakai A, Sobue G (2013) Heat shock factor-1 influences pathological lesion distribution of polyglutamine-induced neurodegeneration. *Nat Commun* 4: 1405

Lalau JD, Lemaire-Hurtel AS, Lacroix C (2011) Establishment of a database of metformin plasma concentrations and erythrocyte levels in normal and emergency situations. *Clin Drug Investig* 31: 435 – 438

Lamb J, Crawford ED, Peck D, Modell JW, Blat IC, Wrobel MJ, Lerner J, Brunet JP, Subramanian A, Ross KN, Reich M, Hieronymus H, Wei G, Armstrong SA, Haggarty SJ, Clemons PA, Wei R, Carr SA, Lander ES, Golub TR (2006) The Connectivity Map: using gene-expression signatures to connect small molecules, genes, and disease. *Science* 313: 1929 – 1935

Li Y, Xu S, Mihaylova MM, Zheng B, Hou X, Jiang B, Park O, Luo Z, Lefai E, Shyy JY, Gao B, Wierzbicki M, Verbeuren TJ, Shaw RJ, Cohen RA, Zang M (2011) AMPK phosphorylates and inhibits SREBP activity to attenuate hepatic steatosis and atherosclerosis in diet-induced insulin-resistant mice. *Cell Metab* 13: 376 – 388

Lin PY, Simon SM, Koh WK, Folorunso O, Umbaugh CS, Pierce A (2013) Heat shock factor 1 over-expression protects against exposure of hydrophobic residues on mutant SOD1 and early mortality in a mouse model of amyotrophic lateral sclerosis. *Mol Neurodegener* 8: 43

Lindquist S (1986) The heat-shock response. *Annu Rev Biochem* 55: 1151 – 1191

Memmott RM, Mercado JR, Maier CR, Kawabata S, Fox SD, Dennis PA (2010) Metformin prevents tobacco carcinogen–induced lung tumorigenesis. *Cancer Prev Res (Phila)* 3: 1066 – 1076

Meng L, Gabai VL, Sherman MY (2010) Heat-shock transcription factor HSF1 has a critical role in human epidermal growth factor receptor-2-induced cellular transformation and tumorigenesis. *Oncogene* 29: 5204 – 5213

Min JN, Huang L, Zimonjic DB, Moskophidis D, Mivechi NF (2007) Selective suppression of lymphomas by functional loss of Hsf1 in a p53-deficient mouse model for spontaneous tumors. *Oncogene* 26: 5086 – 5097

Morimoto RI (2008) Proteotoxic stress and inducible chaperone networks in neurodegenerative disease and aging. *Genes Dev* 22: 1427 – 1438

Mu J, Brozinick JT Jr, Valladares O, Bucan M, Birnbaum MJ (2001) A role for AMP-activated protein kinase in contraction- and hypoxia-regulated glucose transport in skeletal muscle. *Mol Cell* 7: 1085 – 1094

Muchowski PJ, Wacker JL (2005) Modulation of neurodegeneration by molecular chaperones. *Nat Rev Neurosci* 6: 11 – 22

O'Connell-Rodwell CE, Mackanos MA, Simanovskii D, Cao YA, Bachmann MH, Schwettman HA, Contag CH (2008) In vivo analysis of heat-shock-protein-70 induction following pulsed laser irradiation in a transgenic reporter mouse. *J Biomed Opt* 13: 030501

Pickart CM, Eddins MJ (2004) Ubiquitin: structures, functions, mechanisms. *Biochim Biophys Acta* 1695: 55 – 72

Pierce A, Podlutskaya N, Halloran JJ, Hussong SA, Lin PY, Burbank R, Hart MJ, Galvan V (2013) Over-expression of heat shock factor 1 phenocopies the effect of chronic inhibition of TOR by rapamycin and is sufficient to ameliorate Alzheimer's-like deficits in mice modeling the disease. *J Neurochem* 124: 880 – 893

Sadeghi N, Abbruzzese JL, Yeung SC, Hassan M, Li D (2012) Metformin use is associated with better survival of diabetic patients with pancreatic cancer. *Clin Cancer Res* 18: 2905 – 2912

Sanchez I, Mahlke C, Yuan J (2003) Pivotal role of oligomerization in expanded polyglutamine neurodegenerative disorders. *Nature* 421: 373 – 379

Santagata S, Mendillo ML, Tang YC, Subramanian A, Perley CC, Roche SP, Wong B, Narayan R, Kwon H, Koeva M, Amon A, Golub TR, Porco JA Jr, Whitesell L, Lindquist S (2013) Tight coordination of protein translation and HSF1 activation supports the anabolic malignant state. *Science* 341: 1238303

Scott KL, Nogueira C, Heffernan TP, van Doorn R, Dhakal S, Hanna JA, Min C, Jaskelioff M, Xiao Y, Wu CJ, Cameron LA, Perry SR, Zeid R, Feinberg T, Kim M, Vande Woude G, Granter SR, Bosenberg M, Chu GC, DePinho RA *et al* (2011) Proinvasion metastasis drivers in early-stage melanoma are oncogenes. *Cancer Cell* 20: 92 – 103

Shackelford DB, Shaw RJ (2009) The LKB1-AMPK pathway: metabolism and growth control in tumour suppression. *Nat Rev Cancer* 9: 563 – 575

Sum CF, Webster JM, Johnson AB, Catalano C, Cooper BG, Taylor R (1992) The effect of intravenous metformin on glucose metabolism during hyperglycaemia in type 2 diabetes. *Diabet Med* 9: 61 – 65

Tomic T, Botton T, Cerezo M, Robert G, Luciano F, Puissant A, Gounon P, Allegra M, Bertolotto C, Bereder JM, Tartare-Deckert S, Bahadoran P, Auberger P, Ballotti R, Rocchi S (2011) Metformin inhibits melanoma development through autophagy and apoptosis mechanisms. *Cell Death Dis* 2: e199

Vingtdeux V, Davies P, Dickson DW, Marambaud P (2011) AMPK is abnormally activated in tangle- and pre-tangle-bearing neurons in Alzheimer's disease and other tauopathies. *Acta Neuropathol* 121: 337 – 349

Viollet B, Guigas B, Sanz Garcia N, Leclerc J, Foretz M, Andreelli F (2012) Cellular and molecular mechanisms of metformin: an overview. *Clin Sci (Lond)* 122: 253 – 270

Walter P, Ron D (2011) The unfolded protein response: from stress pathway to homeostatic regulation. *Science* 334: 1081 – 1086

Wang X, Khaleque MA, Zhao MJ, Zhong R, Gaestel M, Calderwood SK (2006) Phosphorylation of HSF1 by MAPK-activated protein kinase 2 on serine 121, inhibits transcriptional activity and promotes HSP90 binding. *J Biol Chem* 281: 782 – 791

Welch WJ (1991) The role of heat-shock proteins as molecular chaperones. *Curr Opin Cell Biol* 3: 1033 – 1038

Westerheide SD, Morimoto RI (2005) Heat shock response modulators as therapeutic tools for diseases of protein conformation. *J Biol Chem* 280: 33097 – 33100

Xiao X, Zuo X, Davis AA, McMillan DR, Curry BB, Richardson JA, Benjamin IJ (1999) HSF1 is required for extra-embryonic development, postnatal growth and protection during inflammatory responses in mice. *EMBO J* 18: 5943 – 5952

Zhou G, Myers R, Li Y, Chen Y, Shen X, Fenyk-Melody J, Wu M, Ventre J, Doebber T, Fujii N, Musi N, Hirshman MF, Goodyear LJ, Moller DE (2001) Role of AMP-activated protein kinase in mechanism of metformin action. *J Clin Invest* 108: 1167 – 1174

Zwicker JI (2010) Impedance-based flow cytometry for the measurement of microparticles. *Semin Thromb Hemost* 36: 819 – 823